Moisture Transport during Large Snowfall Events in the New Zealand Southern Alps: The Role of Atmospheric Rivers

RASOOL PORHEMMAT,[a,b] HEATHER PURDIE,[a] PEYMAN ZAWAR-REZA,[a] CHRISTIAN ZAMMIT,[b] AND TIM KERR[c]

[a] *School of Earth and Environment, University of Canterbury, Christchurch, New Zealand*
[b] *National Institute of Water and Atmospheric Research, Christchurch, New Zealand*
[c] *Rainfall.NZ, Christchurch, New Zealand*

(Manuscript received 15 February 2020, in final form 31 October 2020)

ABSTRACT: Synoptic-scale moisture transport during large snowfall events in the New Zealand Southern Alps is largely unknown due to a lack of long-term snow observations. In this study, records from three recently developed automatic weather stations (Mahanga, Mueller Hut, and Mt Larkins) near the Main Divide of the Southern Alps were used to identify large snowfall events between 2010 and 2018. The large snowfall events are defined as those events with daily snow depth increase by greater than the 90th percentile at each site. ERA-Interim reanalysis data were used to characterize the hydrometeorological features of the selected events. Our findings show that large snowfall events in the Southern Alps generally coincide with strong fields of integrated vapor transport (IVT) within a northwesterly airflow and concomitant deepening low pressure systems. Considering the frequency of large snowfall events, approximately 61% of such events at Mahanga were associated with narrow corridors of strong water vapor flux, known as atmospheric rivers (ARs). The contributions of ARs to the large snowfall events at Mueller Hut and Mt Larkins were 70% and 71%, respectively. Analysis of the vertical profiles of moisture transport dynamics during the passage of a landfalling AR during 11–12 October 2016 revealed the key characteristics of a snow-generating AR in the Southern Alps. An enhanced presence of low- and midlevel moisture between 700 and 850 hPa and pronounced increases of wind velocities (more than 30 m s^{-1}) with high values of the meridional component between 750 and 850 hPa were identified over the Southern Alps during the event.

KEYWORDS: South Pacific Ocean; Atmospheric circulation; Snowfall; Hydrometeorology

1. Introduction

In midlatitudes a sizeable fraction of moisture is transported through atmospheric rivers (AR) (Neiman et al. 2008a; Ralph et al. 2004). ARs are narrow channels of enhanced water vapor within the atmosphere that are responsible for most horizontal transport of moisture outside of the tropics (Zhu and Newell 1998; Ralph et al. 2019). In the hydrometeorological literature, other terms such as warm conveyor belt (WCB) and tropical moisture exports (TMEs) are also used to define similar mesoscale and synoptic-scale features with high water vapor content impacting the hydrological cycle in many parts of the world (Gimeno et al. 2014; Ralph et al. 2017). However, TMEs are characterized by high horizontal export of tropical moisture content to higher latitudes (Lu and Lall 2016), and WCB are defined as cyclonic-relative airflows as strongly ascending in the vicinity of extratropical cyclones and their fronts (Eckhardt et al. 2004). Although the term "atmospheric rivers" was first used by Zhu and Newell (1998), knowledge about these filamentary plumes of enhanced moisture in the lower troposphere has been known for a while (Gimeno et al. 2014). The word "rivers" was used as an analogy of the filamentary water flux to that within the world's largest rivers (Gimeno et al. 2014; Newell et al. 1992). Nontechnical terms such as "Pineapple Express," "Hawaiian fire hose," and "Maya Express" are commonly synonymous to this phenomenon in North America (Dirmeyer and Kinter 2009; Lackmann and Gyakum 1999). More than 90% of total water vapor flux at midlatitudes is found to be associated with ARs (Zhu and Newell 1998; Neiman et al. 2008a). The two main sources of moisture in ARs are local moisture convergence along the cold front of an extratropical cyclone and the direct poleward transport of tropical moisture (Bao et al. 2006).

The high moisture content and strong wind velocities associated with ARs usually bring about heavy precipitation, especially when they intercept mountain terrains (Neiman et al. 2013; Ralph et al. 2004; Rutz et al. 2014; Junker et al. 2008; Guan et al. 2010). Strong relationships have been found between ARs and hydrological processes such as precipitation, streamflow and flooding events in the midlatitudes of western North America (Ralph et al. 2016; Neiman et al. 2008b; Guan et al. 2010; Dettinger et al. 2011; Neiman et al. 2008a; Leung and Qian 2009), South America (Viale and Nuñez 2011; Viale et al. 2018; Molero and Novelli 2019), and Europe (Stohl et al. 2008; Whan et al. 2020; Lavers et al. 2012; Lavers and Villarini 2013; Benedict et al. 2019). In the western United States, for example, it is estimated that 25%–50% of the total water supply in California is due to the landfall of ARs (Guan et al. 2010; Dettinger et al. 2011). One of the reasons ARs have recently gained more attention in regions such as western United States is their potential to put an end to long-term droughts. About 33%–40% of the drought breaks in California are related to the landfall of atmospheric rivers (Dettinger 2013).

At higher altitudes, ARs have been found to be an important source of solid precipitation in the Sierra Nevada, the Andes,

Corresponding author: Rasool Porhemmat, rasool.porhemmat@pg.canterbury.ac.nz

DOI: 10.1175/JHM-D-20-0044.1

and Antarctica (Guan et al. 2010, 2013, 2012; Hansen et al. 2013; Demaria et al. 2017; Huning et al. 2017, 2019). Satellite measurements and in situ observations in the western United States show that up to 40% of seasonal snow water equivalent are the result of ARs (Guan et al. 2010). Frequent landfalls of ARs accompanied by the negative phases of the Arctic Oscillation (AO) and the Pacific–North American (PNA) atmospheric circulation indices provide conditions favorable for anomalously high snow accumulation across the Sierra Nevada (Guan et al. 2013). The penetration of ARs to the inland semiarid Southwest of the United States can lead to a contribution of more than 25% of winter precipitation (Demaria et al. 2017). The analysis of three historic snowstorms during the past 60 years on Mt. Shasta, in California, United States, demonstrated a clear link between large snowfall events and ARs (Hansen 2016). Investigation of climatology of winter precipitation over the subtropical central Andes indicates that strong water vapor transport from the Pacific Ocean largely modulates heavy snowfall events in the region (Viale and Nuñez 2011). In the southern Andes, Saavedra et al. (2020) reported that around 51% of total snow accumulation is the result of ARs. Similarly, Gorodetskaya et al. (2014) reported a close connection between extreme snowfall events and strong moisture fluxes associated with ARs in East Antarctica where a large portion of annual snow accumulation is found to be linked to few extreme snowfall events.

Moisture transport in the South Pacific region across the Tasman Sea enhanced by regional orographic influence is a typical feature of winter precipitation in the Southern Alps (Little et al. 2019; Cullen et al. 2019). However, the contribution of ARs in climate and hydrometeorology of the Southern Alps is limited. This is surprising given that recent global studies have shown that a considerable number of ARs occur in the New Zealand region (Waliser and Guan 2017; Guan and Waliser 2015). Recently Kingston et al. (2016) investigated the impact of ARs on extreme flooding events at the Waitaki River between 1972 and 2012, finding that all major flooding events were associated with ARs. Their study highlighted the need for further investigation to better understand the role of ARs in the region. More recently, Little et al. (2019) documented the role of ARs on glacier mass balance at Brewster glacier, located on the west side of the Main Divide of the Southern Alps, showing significant relationship between ARs and glacier mass gain and loss by influencing snow accumulation and snow ablation. It is, therefore, important to examine the role of ARs on large snowfall events at a greater spatial scale across the Southern Alps.

Given the importance of westerly and northwesterly airflow for Southern Alps precipitation (Henderson and Thosmson 1999; Griffiths and Mcsaveney 1983; Little et al. 2019; Purdie et al. 2011), of particular interest is the analysis of moisture transport in the South Pacific region over the Tasman Sea and its relationship with large snowfall events in the Southern Alps. Large snowfall events are a critical source of water in mountain catchments by increasing total snow water equivalent (SWE). The Southern Alps form the headwaters of most of the rivers in the South Island. Seasonal snow is an important element of water resources in the Southern Alps by influencing the timing and magnitude of the discharge of alpine rivers (Clark et al. 2009; Kerr 2013). Meltwater from seasonal snowpacks can contribute up to 40%–50% of the discharge in upper alpine catchments which in turn feed major rivers in the Southern Alps (Fitzharris and Garr 1995; Sirguey 2009). This contribution impacts the hydroelectricity generation capability and sustainable irrigation during summer (Hendrikx et al. 2012; McKerchar et al. 1998; Thompson 2002). However, climate change is expected to substantially impact the seasonal snowpacks in the Southern Alps (Hendrikx et al. 2012; Poyck et al. 2011; Jobst et al. 2018).

Regional climate models currently suggest that the maximum daily temperatures in the Southern Alps of New Zealand could rise by more than 4°C by the end of this century (Dean et al. 2006). Improved understanding of the atmospheric dynamics and moisture transport controlling the timing and magnitude of snowfall will provide important information for water management policies in the region, given the potential impact of climate change on the distribution and duration of seasonal snowpacks in the Southern Alps. The main objective of this study is to explore the key characteristics of moisture flux during large snowfall events in the region. Gridded atmospheric reanalysis data and daily snow observations across the Southern Alps are used to assess the contribution of ARs to such events by analyzing the magnitudes of integrated vapor transport (IVT) during snowstorms.

2. Data and methodology

a. Data sources

Snow observations were obtained from the Snow and Ice Monitoring Network (SIN). SIN is a network of high-altitude automatic weather stations (AWS) established by New Zealand National Institute of Water and Atmospheric Research (NIWA). Three SIN sites, namely, Mahanga, Mueller Hut, and Mt Larkins (Fig. 1) were selected because of their spatial distribution across the Southern Alps providing coverage of the north, middle, and southern portions of the Southern Alps. All three sites are located in the upper terrains of the Southern Alps close to the Main Divide at relatively high altitudes (Mahanga: 1955 m, Mueller Hut: 1818 m, Mt Larkins: 1900 m). Continuous records of snow depth measurements are available since 2009 at Mahanga, 2010 at Mueller Hut, and 2014 at Mt Larkins.

To identify daily snowfall events, snow depth observations recorded by an ultrasonic depth gauge (SR50) were used. Only daily snowfall events with depths greater than 2.5 mm, which is the precision of the recorded data, were considered at each station. In hydrological studies the threshold used to determine large or extreme events such as precipitation, or flooding is mostly based on percentile-based indices, for example, using the percentile values of >90th, >95th, >99th, and >99.9th (Vicente-Serrano et al. 2017; Lute and Abatzoglou 2014). Different thresholds of daily snowfall ranging from 5 to 33 cm of daily snow depth increase have been used in previous studies to determine large snowfall events (see Birkeland and Mock 1996; Bednorz 2011; Merino et al. 2014; Bednorz and Wibig 2016). Snowfall varies spatially and temporally across the Southern Alps (Kerr et al. 2013; Webster et al. 2015; Clark et al. 2011;

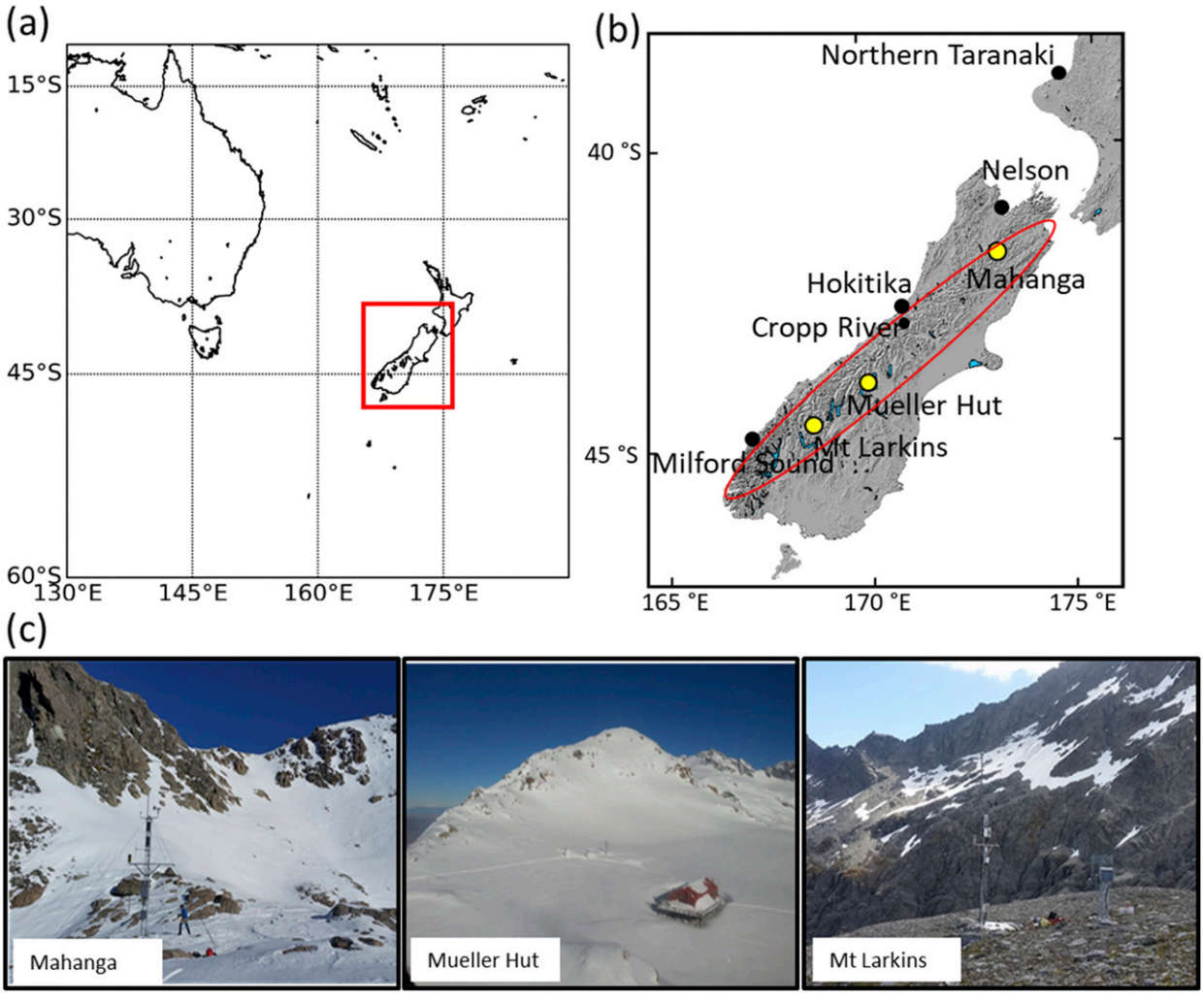

FIG. 1. (a) Synoptic window over South Pacific region used in this study (10°–60°S and 130°E–160°W), (b) locations of automatic weather stations (yellow dots) in the Southern Alps, and (c) photos of three study sites. Photo credits: NIWA's field team.

Purdie et al. 2011); therefore, a single threshold cannot be used to identify large events over the region. For the purpose of this study, the selection of large events was based on 24-h snow depth increase by greater than the 90th percentile at each site over the period of observation. In the case where large snowfall events were associated with snowstorms longer than 24 h, analysis was conducted for the total period of the storm rather than individual snowfall days.

The meteorological fields were obtained from the European Centre for Medium-Range Weather Forecasts (ECMWF) interim reanalysis (ERA-Interim) data (Dee et al. 2011). Meteorological observations on land and ocean are assimilated into numerical weather prediction models to produce atmospheric reanalysis data (Lavers et al. 2012). ERA-Interim data were retrieved at 6-hourly temporal resolution and 0.5° × 0.5° spatial resolution for a geographic window spanning of 10°–60°S and 130°E–160°W (see Fig. 1b). The data used in this study include sea level pressure (SLP; hPa), geopotential height at 500 hPa (Z500; m), temperature (T; °C), specific humidity (q; g kg^{-1}), specific cloud ice water content (g kg^{-1}), zonal and meridional wind fields (u and v; m s^{-1}), vertical integral of cloud frozen water flux (VICFWF; kg m^{-1} s^{-1}), and vertical integral of liquid water flux (VICLWF; kg m^{-1} s^{-1}).

b. *Moisture transport: Identification of ARs*

The total amount of water in the atmosphere provides critical information about moisture transport from tropics to midlatitudes (Schumacher et al. 2020; Lavers et al. 2012; Dettinger et al. 2011; Rutz et al. 2014). There are two commonly used methods to quantify intense lower-tropospheric moisture. The first approach measures the IVT (kg m^{-1} s^{-1}) and the second approach measures integrated water vapor (IWV; cm). IVT is defined as

$$\mathrm{IVT} = \sqrt{\left(\frac{1}{g}\int_{1000\,\mathrm{hPa}}^{300\,\mathrm{hPa}} qu\,dp\right)^2 + \left(\frac{1}{g}\int_{1000\,\mathrm{hPa}}^{300\,\mathrm{hPa}} qv\,dp\right)^2}, \quad (1)$$

where g ($\mathrm{m\,s^{-2}}$) is the gravitational acceleration, q ($\mathrm{g\,Kg^{-1}}$) is the specific humidity, u ($\mathrm{m\,s^{-1}}$) is the zonal component of the wind, v ($\mathrm{m\,s^{-1}}$) is the meridional component of the wind, and p is the pressure. IWV is defined as

$$\mathrm{IWV} = \frac{1}{g}\int_{1000\,\mathrm{hPa}}^{300\,\mathrm{hPa}} q\,dp, \tag{2}$$

where g ($\mathrm{m\,s^{-2}}$) is the gravitational acceleration and q ($\mathrm{g\,K\,g^{-1}}$) is the specific humidity. The merit of the use of AR detection algorithms to study the moisture transport is the relative simplicity of finding the filamentary patterns of water vapor associated with this phenomenon as well as simple identification of the role of ARs in the hydrological cycle at a regional and global scale (Gimeno et al. 2014; Hansen 2016; Rutz et al. 2019). In most recent hydrometeorological studies IVT is preferred over IWV for identifying ARs (Young et al. 2017; Ralph et al. 2019; Waliser and Guan 2017; Cordeira et al. 2017). This is mainly because IVT has a better relationship with precipitation over mountainous terrains (Junker et al. 2008; Guan et al. 2013), and a stronger correlation with winter precipitation (Rutz et al. 2014; Guan et al. 2013, 2016, 2010). The IVT prior and during the snowfall events was computed for the synoptic window of 10°–60°S and 130°E–160°W (Fig. 1a). The integration was conducted on specific humidity and u and v components of the wind for 50-hPa intervals between 300 and 1000 hPa using Eq. (1).

This study followed the approach taken by Rutz et al. (2014) where areas with IVT greater than a specific threshold (e.g., 100 or 250 $\mathrm{kg\,m^{-1}\,s^{-1}}$), longer than 2000 km in length, and with length/width (L/w) ratio of greater than 2 are identified as ARs. Most AR detection algorithms are based on employing IVT thresholds (e.g., Neiman et al. 2008a; Dettinger et al. 2011; Gimeno et al. 2014). The 85th percentile of IVT values have been used in several studies conducted in midlatitudes of Europe and North America (Guan and Waliser 2015; Lavers et al. 2012; Shields et al. 2018; Rutz et al. 2019), and this is the approach used here. We calculate the 6-hourly IVT values for a grid point located on the west coast of South Island approximately between 40.5° and 46°S (Figs. 2a,b) during the main snow accumulation months in the Southern Alps (June–October 2009–17). The selection of IVT threshold ($232.6\,\mathrm{kg\,m^{-1}\,s^{-1}}$) during snow accumulation months is because considerable differences in the values of IVT have been reported for different seasons in midlatitude regions (Guan and Waliser 2015; Lavers et al. 2012). Next we calculate the average IVT over the course of each snowfall event on the west coast of South Island at the closest grid point to each snow observation (Mahanga: 41.5°S, 171°E; Mueller Hut: 43.5°S, 169°E; Mt Larkins: 44.5°S, 167°E). If the average IVT during each snowfall event exceeds the threshold, the moisture flux will be checked for the shape requirements ($L \geq 2000$ km and $L/w \geq 2$).

In addition to analysis of IVT, in order to obtain more information about the moisture transport during the days leading to the snowfall events, the average values of ERA-Interim VICFWF and VICLWF ($\mathrm{kg\,m^{-1}\,s^{-1}}$) are calculated. These two variables reveal the relative amounts of solid or liquid water in the clouds (Daniel et al. 2002) which largely influences precipitation in mountainous regions by impacting the seeder–feeder phenomenon (Khain and Pinsky 2018).

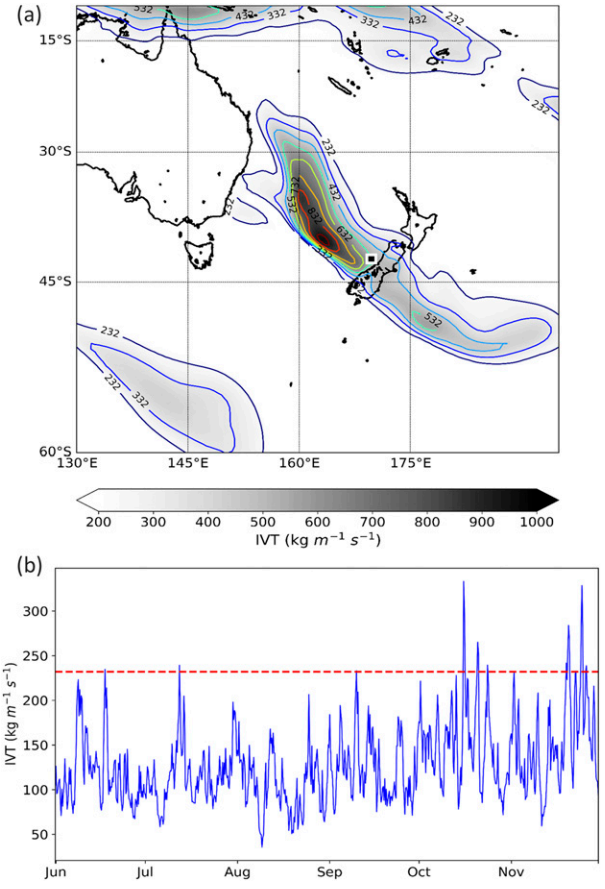

FIG. 2. (a) A detected AR over South Island of New Zealand. The black square marks the location of the grid point at which the 85th percentile IVT was calculated. (b) Time series of average IVT for the period of 2009–17 along the west coast of New Zealand's South Island (43°S, 170.5°E). The red dashed line represents the 85th percentile of IVT value ($232\,\mathrm{kg\,m^{-1}\,s^{-1}}$).

3. Results

a. *Large snowfall events in the Southern Alps*

Measurements of snow depth over the course of this study reveal that snowfall events can occur throughout the year in the Southern Alps. However, at Mahanga, the most northern station, snow mainly accumulates from June to September, reaching a peak in September (Fig. 3a). At Mueller Hut and Mt Larkins sites the snow accumulation season is slightly longer, ending in October, with a maximum accumulation between mid-September to early October (Figs. 3b,c). Snowmelt, however, occurs over a relatively shorter period in the Southern Alps. At Mueller Hut and Mt Larkins the snowmelt period is usually between mid-October and mid-December, while at Mahanga seasonal snowpack melts from approximately late September to mid-November. The 90th percentile of daily snow depth led to selecting a threshold of 12.5 cm of daily snow for

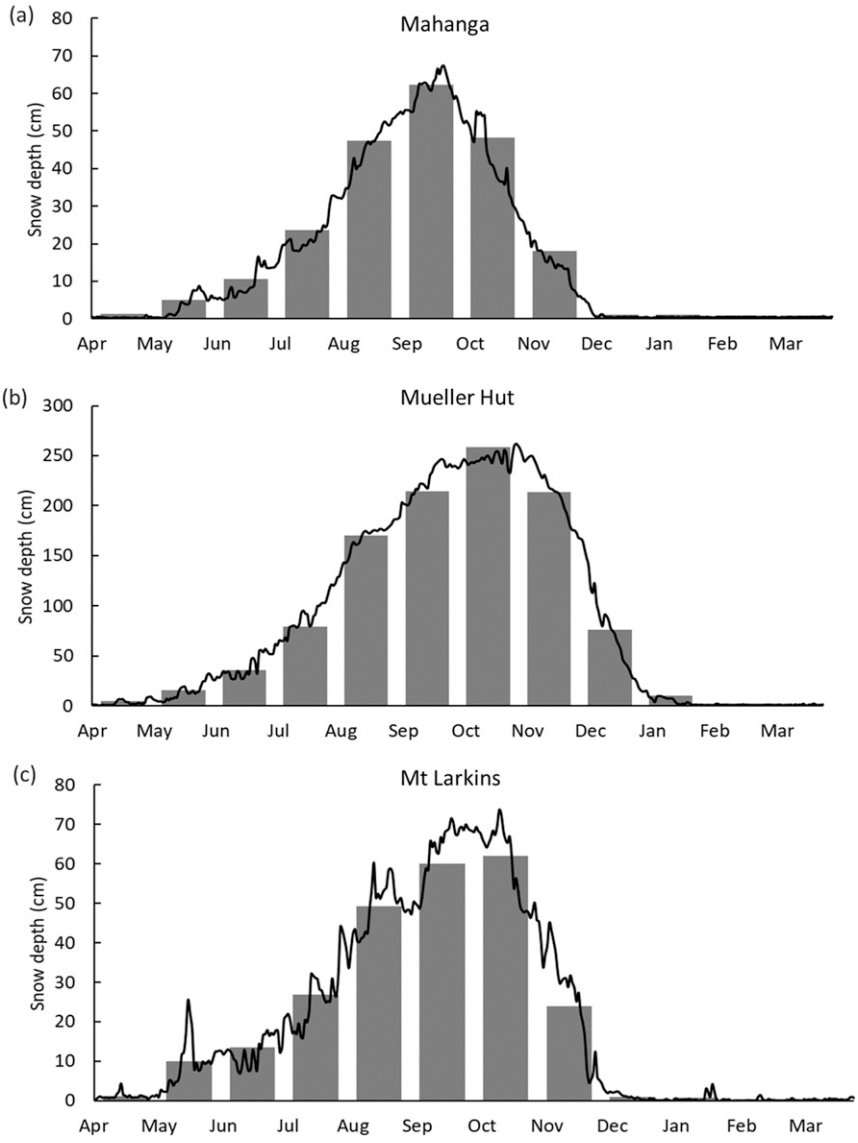

FIG. 3. The average daily (lines) and monthly (bar charts) snow accumulation at (a) Mahanga (2009–17), (b) Mueller Hut (2010–17), and (c) Mt Larkins (2014–17).

Mahanga, 18 cm for Mt Larkins, and 31 cm for Mueller Hut for detecting large snowfall events. This amounted to 21 events at Mahanga, 17 events at Mueller Hut, and 14 events at Mt Larkins (Table 1). The proportion of the average annual sum of large snowfall events relative to the total snow accumulation indicates that an average of 26% (Mahanga), 32% (Mueller Hut), and 28% (Mt Larkins) of the interannual variability in snow depth were associated with these events. In the winter of 2016/17, approximately 40% of annual snow accumulation recorded at Mueller Hut was received during only six large snowfall events.

b. Association of ARs with large snowfall events

Figure 4 shows the average values of 6-hourly IVT, VICFWF, and VICLWF during the large snowfall events. The mean estimates of VICFWF and VICLWF during the snowfall events were used to diagnose the importance of the moisture content in the clouds during the snowfall events. Figure 4a reveals that over the period of snowstorms VICFWF increased toward the Southern Alps where the highest values of VICFWF were calculated for the grid points of three snow observation sites near the Main Divide ($2.8\,kg\,m^{-1}\,s^{-1}$ at Mahanga, $3.4\,kg\,m^{-1}\,s^{-1}$ at Mueller Hut, and $3.3\,kg\,m^{-1}\,s^{-1}$ at Mt Larkins). The average values of VICLWF shows a similar pattern to VICFWF; however, the liquid water flux decreases from the west coast toward the Southern Alps with the higher values recorded on the west coast of the South Island ($3.9\,kg\,m^{-1}\,s^{-1}$ at Mahanga, $5.4\,kg\,m^{-1}\,s^{-1}$ at Mueller Hut, and $4.7\,kg\,m^{-1}\,s^{-1}$ at Mt Larkins, Fig. 4b). Depicting the average values of 6-hourly IVT during the large snowfall, Fig. 4c shows relatively high moisture flux (greater than IVT 85th percentile: $232\,kg\,m^{-1}\,s^{-1}$)

TABLE 1. Snow depth observations and IVT magnitudes during large snowfall events at three SIN sites (Mahanga, Mueller Hut, and Mt Larkins).

Event	Duration (h)	SD (cm)	Max IVT alongside west coast	Average IVT alongside west coast	Max IVT at SIN sites	$L/W \geq 2$	AR: yes/no
			Mahanga				
9 Jun 2009	12	14.1	390	170.7	242.2	✓	No
3 Jul 2009	18	12.7	363.8	187.9	194.9	✓	No
23–24 Jul 2009	22	42.0	476	314.4	362.7	✓	Yes
31 Aug 2009	16	12.7	600.6	410.7	443.3	✓	Yes
8 Jun 2010	22	18.8	540.9	322.6	369.1	✓	Yes
9–10 Nov 2010	24	16.7	359.5	247.3	265.9	✓	Yes
20 Oct 2010	13	13.8	225.8	176.9	195.0	×	No
18 Jun 2012	19	15.0	402.1	288.3	324.1	✓	Yes
9 Sep 2012	34	18.2	664.9	403.3	487.7	✓	Yes
8 Aug 2013	14	14.2	319.8	245.5	263.2	✓	Yes
12–13 Aug 2014	18	29.0	461.8	261.9	353.4	✓	Yes
16–17 Sep 2014	28	17.1	289.1	179.2	198.3	×	No
20 Sep 2014	18	17.0	273.9	199.3	225.9	✓	No
12 Nov2014	25	14.0	392.8	254.7	329.8	✓	Yes
19 Nov 2014	18	14.3	309.3	222.9	251.6	✓	No
20 May 2016	21	14.6	464.6	281.8	326.1	×	No
21 Jun 2016	24	31.9	513.2	382.8	263.6	✓	Yes
3 Jul 2016	19	13.7	310.4	221.1	146.1	×	No
26–27 Jul 2016	37	27.0	403.6	245.1	276.9	✓	Yes
14 Aug 2017	12	21.3	360.2	284.4	297.5	✓	Yes
7 Sep 2017	16	26.9	320.19	242.2	265.5	✓	Yes
Contribution of large snowfall events to the total annual snow accumulation: 26%							
Contribution of ARs to large snowfall events: 61% (13 events)							
			Mueller Hut				
25 Sep 2010	19	30.3	377.7	307.7	338.8	✓	Yes
18–19 Oct 2011	32	49.5	321.8	245.2	356.6	✓	Yes
2–3 Aug 2014	29	74.7	441.7	269.9	424.9	✓	Yes
12–13 Aug 2014	18	32.5	269.3	203.1	340.9	×	No
15–16 Sep 2014	24	35.2	177.6	150.9	178.8	×	No
19–20 Nov 2014	27	32.4	362.1	254.8	294.6	✓	Yes
1–2 Sep 2015	26	32.3	435.0	345.1	296.2	✓	Yes
13–14 Jul 2016	28	99.0	542.2	366.3	556.8	✓	Yes
24 Jul 2016	21	32.8	525.4	299.9	511.0	✓	Yes
28–29 Jul 2016	34	31.1	238.2	152.5	189.8	×	No
11–12 Oct 2016	18	70.0	485.9	355	478.0	✓	Yes
12 Oct 2016	22	30.9	88.5	65.7	79.5	×	No
26–27 Nov 2016	46	35.5	332.0	269.2	274.0	✓	Yes
1–2 Jul 2017	32	81.3	368.1	237.4	366.6	✓	Yes
22 Jul 2017	26	51.4	369.4	319.9	452.7	✓	Yes
13–14 Aug 2017	32	33.0	330.2	236.6	240.1	×	No
5–6 Sep 2017	34	63.0	280.0	237.0	276.9	✓	Yes
Contribution of large snowfall events to the total annual snow accumulation: 32%							
Contribution of ARs to large snowfall events: 70% (12 events)							
			Mt Larkins				
1 Jul 2014	20	34.0	520.4	319.0	425.9	✓	Yes
11 Aug 2014	18	29.9	410.8	231.6	78.4	×	No
14–15 May 2015	32	46.5	360.3	262.8	286.9	×	No
15 Jun 2015	22	33.9	317.3	281.0	273.7	✓	Yes
18 Jun 2015	18	24.6	508.3	326.0	404.5	✓	Yes
19 Aug 2015	19	19.6	367.2	268.4	269.8	✓	Yes
13–14 Jul 2016	34	67.0	541.0	301.1	398.6	✓	Yes
27–28 Jul 2016	34	59.5	302.4	264.0	271.3	×	No
11–12 Oct 2016	24	108.0	570.8	374.6	495.4	✓	Yes
26–27 Nov 2016	24	27.0	504.3	276.9	325.1	✓	Yes
13 Aug 2017	22	29.5	372.2	258.1	256.3	✓	Yes
5–6 Sep 2017	28	23.8	355.5	264.5	245.9	✓	Yes
9 Sep 2017	18	32.7	242.2	153.9	218.1	×	No
5 Nov 2017	14	25.9	366.4	280.3	255.8	✓	Yes
Contribution of large snowfall events to the total annual snow accumulation: 28%							
Contribution of ARs to large snowfall events: 71% (10 events)							

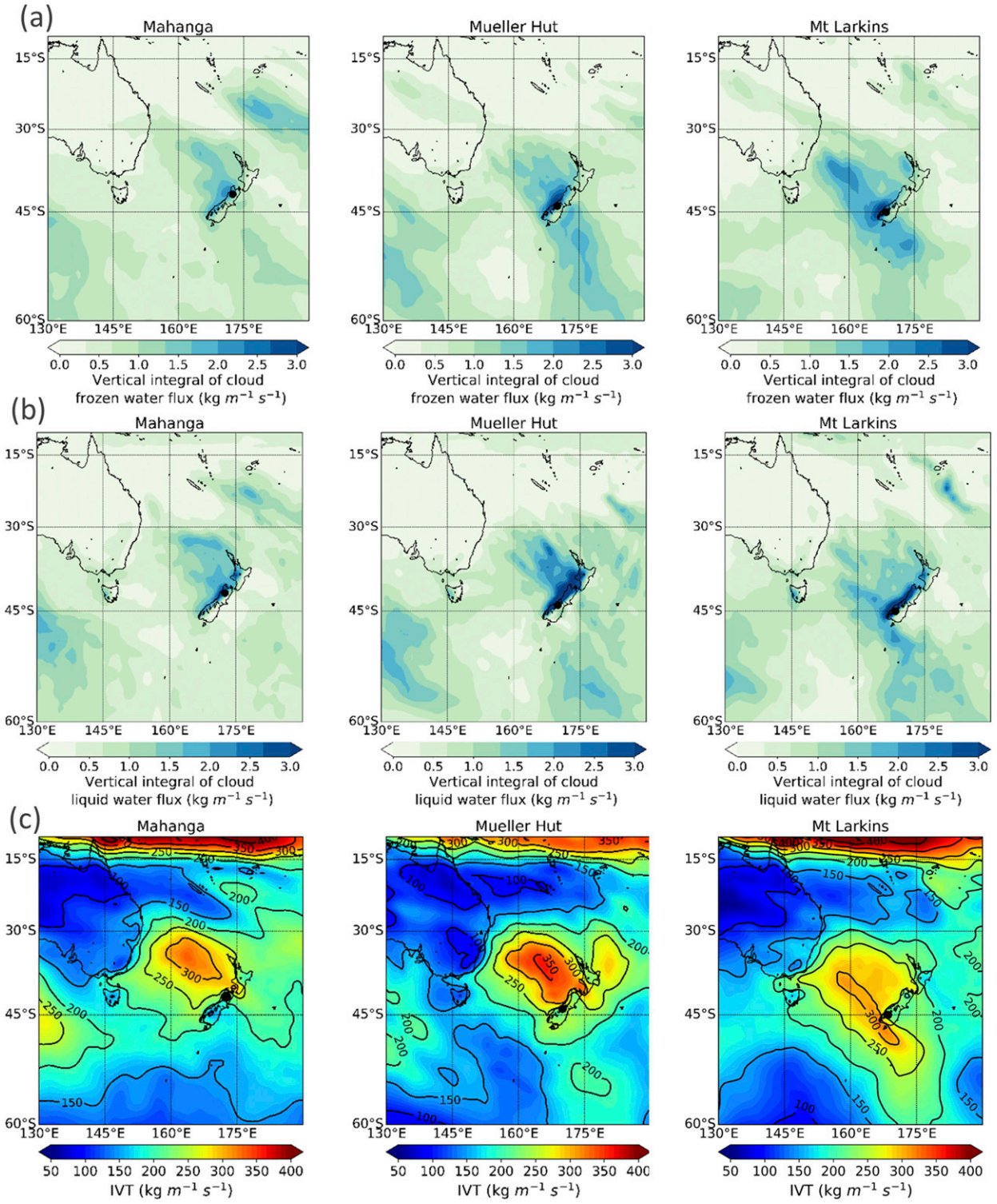

FIG. 4. (a) Average VICFWF (kg m^{-1} s^{-1}), (b) average VICLWF (kg m^{-1} s^{-1}), and (c) average IVT (kg m^{-1} s^{-1}). The average values are calculated during large snowfall events at Mahanga (2009–2017), Mueller Hut (2010–17), and Mt Larkins (2014–17).

along the west coast of South Island. The average IVT is within the range of 260–300 kg m^{-1} s^{-1} over the period of the snowstorms (260 kg m^{-1} s^{-1} at Mahanga, 290 kg m^{-1} s^{-1} at Mueller Hut, and 275 kg m^{-1} s^{-1} at Mt Larkins).

As the main focus of this study is the assessment of moisture transport for each individual storm, the key characteristics of moisture flux during the identified large snowfall events have been explored. Table 1 summarizes the details of IVT calculations, the requirements for AR identification as well as duration and total accumulated snow depth during the events. Three examples of identified landfalling ARs responsible for large snowfall events at the three locations are shown in Fig. 5. These three ARs resulted in the largest snowfall event recorded at each location (see Table 1). Despite considerable snowfall events at high altitudes, these ARs brought about rainfall alongside the coastal regions. During 13–14 July 2016, for example, when the snowstorm dominated the majority of the upper terrains of the Southern Alps (e.g., ~99 cm of snowfall at Mueller Hut, see Table 1), coastal regions such as Northern Taranaki (southwest of North Island, Fig. 1) received considerable rainfall up to 225 mm during the passage of the AR over a period of less than 36 h (Brandolino 2016a). Weather stations on the western South Island recorded heavy rainfalls when the AR made landfall over the region (e.g., 200 mm at Hokitika Gorge and 430 mm at Cropp River). Likewise, during the June 2009 and October 2016 snowstorms, heavy rainfall events (more than 100 mm day^{-1}) was recorded on the west coast of the South Island (Brandolino 2016b).

In terms of magnitude, the analysis of IVT during the landfall of ARs alongside the west coast of the south Island reveals maximum instantaneous values greater than 500 kg m^{-1} s^{-1} during the snowstorms over the Southern Alps (e.g., 9 September 2012 event at Mahanga, 13–14 July 2016 event at Mueller Hut, and 11–12 October at Mt Larkins). However, the average values of IVT over the period of each snowstorm remains mainly below 300 kg m^{-1} s^{-1}. Also, near the Main Divide of the Southern Alps, where the snow observation sites are located, rarely does the maximum IVT exceed 500 kg m^{-1} s^{-1}. Our results show that, considering the frequency of large snowfall events reported in Table 1, approximately 61% of large snowfall events at Mahanga (13 out of 21 events) were associated with ARs. The contributions of ARs to the large snowfall events at Mueller Hut and Mt Larkins were 70% (12 out of 17 events) and 71% (10 out of 14), respectively. However, based on the snow depth increase these proportions are 71%, 80%, and 70% for Mahanga, Mueller Hut, and Mt Larkins, respectively. It is worth noting that from a hydrological perspective it would have been desirable to calculate these contributions based on snow water equivalent rather than snow depth. However, due to lack of reliable and consistent snow water equivalent data during all snowfall events our analysis was limited to snow depth observations. These findings still provide some insight into the potential importance of such narrow channels of moisture to large snow events in the maritime Southern Alps, where up to 40% the total snow accumulation could result from several snowfall events.

c. *Case study: October 2016 event*

To better understand the hydrometeorological characteristics of large snowfall events, a case study of a landfalling AR in

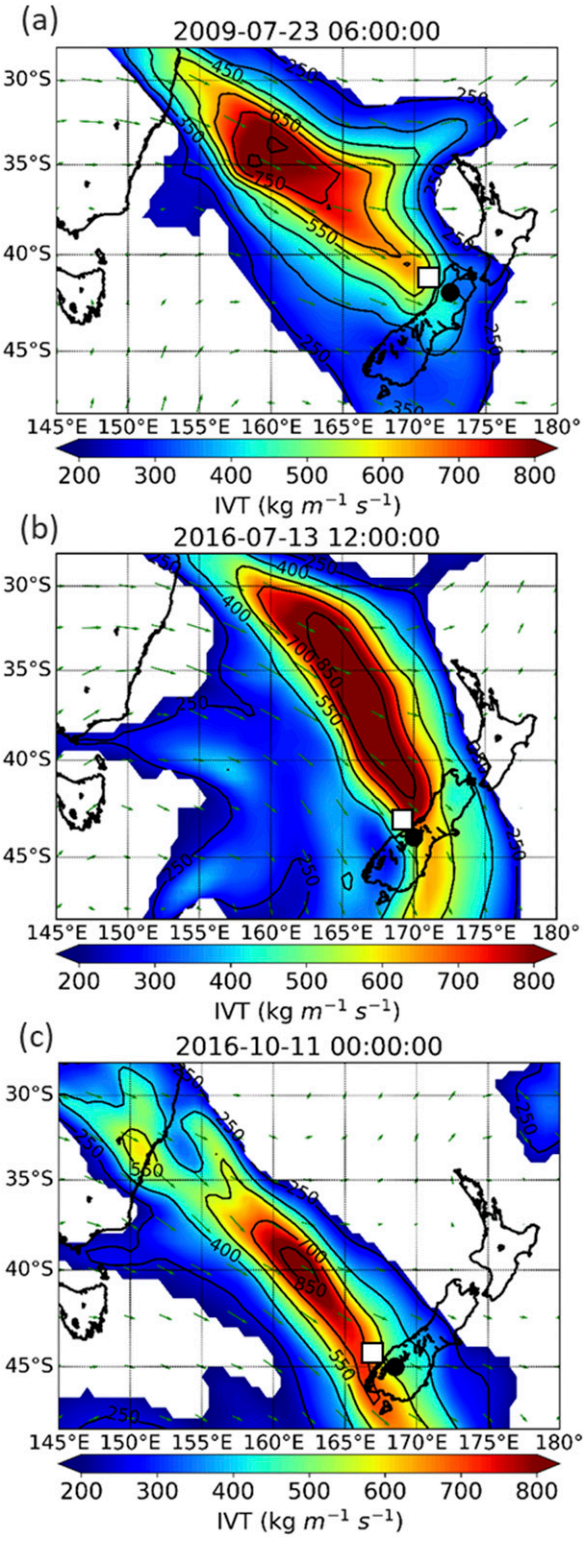

FIG. 5. Examples of ARs during large snowfall events at (a) Mahanga, (b) Mueller Hut, and (c) Mt Larkins. The black dots mark the locations of snow observation sites, and the white squares mark the locations of the closest grid point on the west coast of New Zealand South Island to each snow observation site. Green arrows indicate the wind vectors at 850 hPa.

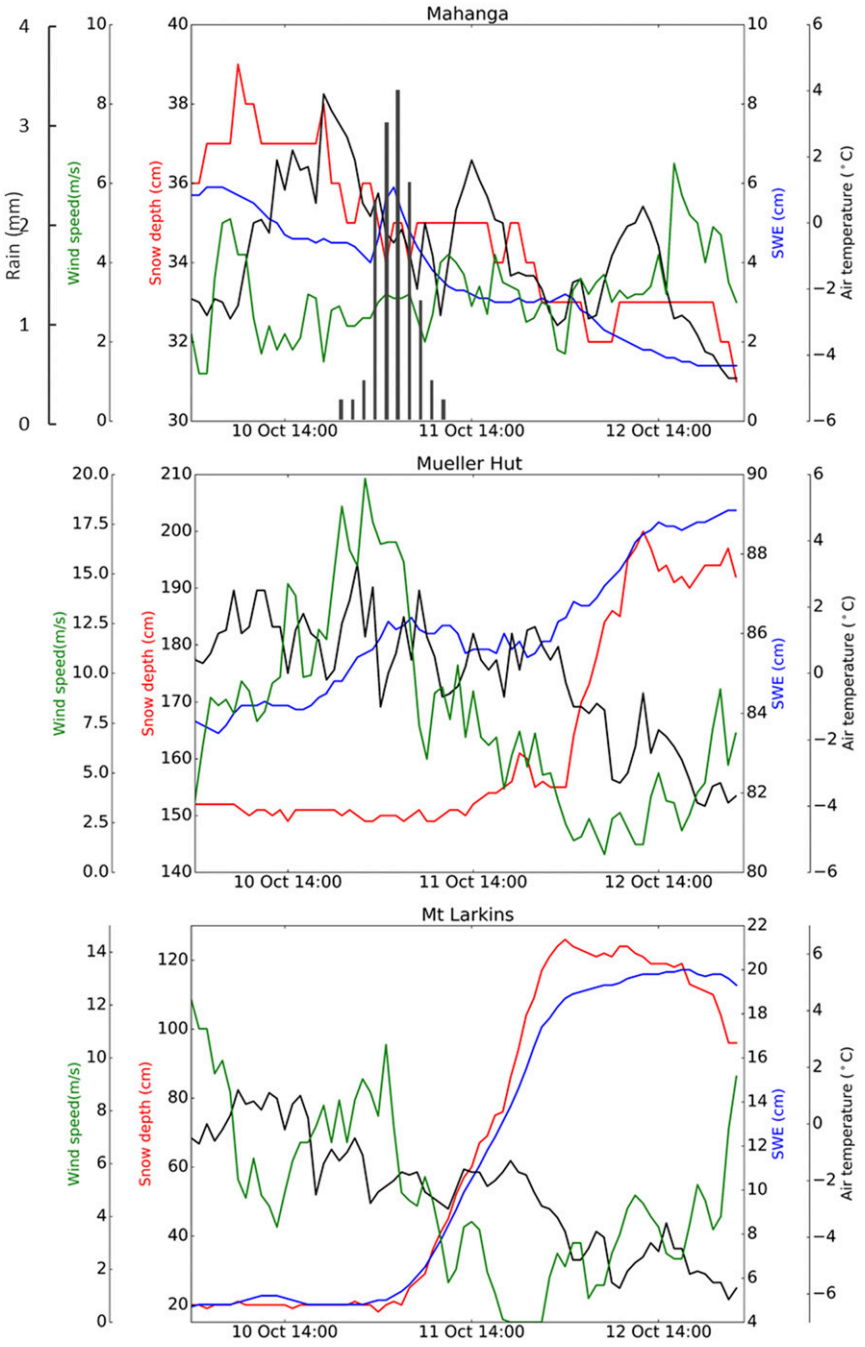

FIG. 6. Hourly hydrometeorological observations recorded at (a) Mahanga, (b) Mueller Hut, and (c) Mt Larkins during October 2016 event.

the Southern Alps is selected for further analysis. The event on the 11–12 October 2016 was chosen because it resulted in considerable snow accumulation at Mt Larkins and Mueller Hut, but liquid precipitation was recorded at Mahanga in the northern part of the Southern Alps. The measurements of snowfall characteristics (SD and SWE) and climate variables (temperature and wind speed) at these locations during the storm are shown in Fig. 6. The event was the largest snowfall event recorded at Mt Larkins with an increase of 108 cm in SD and 17.2 cm in SWE over the period of the storm. Heavy snowfall resulted in road closures of some alpine roads in central and southern parts of South Island. Observations at Mueller Hut show an initial increase in SWE without increasing SD. Even though the rain gauge did not record any measurable precipitation at this stage, relatively higher air temperatures (above 0°C) suggest that this increase in SWE

could be attributed to a short period of rainfall due to warmer airmasses over the Southern Alps ahead of the frontal passages and before snow started falling. Strong wind velocities (up to 19.8 m s^{-1}) could also explain a potential undercatch of liquid precipitation by the rain bucket. Overall, Mueller Hut site received 70 cm of total accumulated snow during the event (Fig. 6b). Despite considerable snow accumulation further south, the AR resulted in rain-on-snow (ROS) conditions at Mahanga with a total accumulated rainfall of 22 mm (Fig. 6a).

HYDROMETEOROLOGICAL CHARACTERISTICS

Analysis of SLP (hPa) and surface temperature T (°C) during the days leading to the snowstorm indicates that the event was the result of a rapidly deepening low pressure system with a central pressure of ~950 hPa near 58°S and 143°E at 0000 New Zealand standard time (NZST) 10 October 2016 (Fig. 7). The cold front, marking the boundary between the colder maritime air mass and the warmer air mass, moved from southwest to northeast toward the South Island. The position of the cold front during the storm seemed to play an important role in determining the type of precipitation over the Southern Alps. While the cold front passes through, northern parts of the Southern Alps remain on the warmer side of the front during 11–12 October.

To further analyze the moisture transport during the storm, the 6-hourly IVT fields were calculated prior and during the event (Fig. 8a). An AR with an exceptionally high moisture flux (core IVT values exceeding 1900 kg m^{-1} s^{-1}) traveled southeastward from the south of Australia. The AR did not initially make landfall alongside the west coast. The spatial distribution and transport of moisture during the days prior to the snowstorm shows the passage of the AR at southern latitudes as it passed the south of the South Island. Afterward, the intense water vapor flux moved northeastward and made landfall over the Southern Alps leading to considerable snow accumulation over the high altitudes of southern and central parts of the Southern Alps. The values of IVT during the passage of the atmospheric river over the three sites are shown in Fig. 8b. A maximum IVT of 500 kg m^{-1} s^{-1} was calculated at Mt Larkins at 0000 NZST 11 October 2016. A similar value of IVT (480 kg m^{-1} s^{-1}) was recorded at the Mueller Hut location at 1200 NZST 11 October 2016. However, the magnitude of IVT decreased as the AR traveled north. Figure 9 shows specific humidity and wind fields over a period of 24 h for three pressure levels (500, 800, 900 hPa). The low- and midtropospheric specific humidity fields show different distribution with an increasing gradient toward the surface. On the west coast of South Island, values more than 6 g kg^{-1} were recorded at 900 hPa. Wind fields at lower and middle troposphere indicate directions perpendicular to the main axis of the Southern Alps as the AR moves over the Southern Alps.

The vertical profiles of specific cloud liquid and ice water content and wind components across the cold fronts during the passage of the ARs over the Southern Alps are given in Fig. 10. The analysis of vertical profiles is conducted to shed more light on the physical processes lying between the synoptic and local scales and characterize the dynamics of moisture transport leading to intense precipitation. The values of specific cloud ice water content showed an increase at middle troposphere at 0000 NZST 11 October 2016 while a distinct rise of specific cloud liquid water was identified between 750 and 900 hPa (Fig. 10a). This coincides with enhanced magnitude of wind velocities below 700 hPa (Fig. 10). The meridional component of the wind at middle and lower levels showed a significant increase reaching a peak of 26 m s^{-1} at 950 hPa. Also, total wind speed values more than 30 m s^{-1} was identified between 850 and 950 hPa. This condition reveals the importance of mid- and low-level jet streams in transporting water vapor from the Pacific Ocean toward the Southern Alps during the event. Somewhat similar conditions can be seen across the cold front over the Southern Alps at 1200 NZST 11 October 2016 when the AR moved toward northeast (Fig. 10b). At this time the cold front was located approximately close to the grid point of Mt Larkins (Fig. 7) when the majority of snow accumulation during the passage of the storm occurred at Mt Larkins and Mueller Hut (Fig. 6).

Another key feature of the AR was an increase in the values of the VICFWF and VICLWF at 0000 NZST 11 October 2016 when AR making landfall across the southern parts of the South Island (Fig. 11). A reduction in VICFWF, representing the ice content of the clouds, was found when the AR moves toward the northern part of the Southern Alps (Figs. 11a,c), while the magnitudes of VICWF, representing the liquid content of cloud, were still relatively high (~20 kg m^{-1} s^{-1}, Fig. 11d). Assessing the temperature characteristics of ARs is essential for evaluating their role in producing snow or rain in the mountains. AR-related storms are generally warm by nature due to warmer vapor airflows originating from tropics (Neiman et al. 2008a; Rössler et al. 2014; Guan et al. 2016). During the October 2016 storm the temperature profile between 300 and 1000 hPa (Fig. 11e) reveals that temperatures at pressure levels above 850 hPa were above 0°C at the grid points of Mueller Hut and Mt Larkins sites at 0000 NZST 11 October 2016, while the freezing level was much higher at Mahanga (~700 hPa). The reduction in cloud ice content and higher freezing level (700 hPa) as the AR move toward northern parts of the Southern Alps provide more evidence as to why the precipitation type shifts from solid to liquid as the AR during the passage of the AR at Mahanga.

4. Discussion

The characteristics of moisture transport during the large snowfall events across the Southern Alps was explored. Data from three SIN sites, distributed along the length of the Southern Alps, have provided valuable observations of the seasonal distribution of snow across the region (Fig. 2). During the large snowfall events in the Southern Alps, enhanced moisture transport with increasing fields of IVT, VICFWF, and VICLWF were identified in the region. The majority of the large snowfall events investigated were found to be associated with ARs and their large-scale water vapor transport across the Tasman Sea. These ARs are transient features at midlatitudes of the Southern Alps with a typical life span of less than 36 h (Table 1). The key role of ARs in winter precipitation of the Southern Alps are in line with previous studies in other parts of

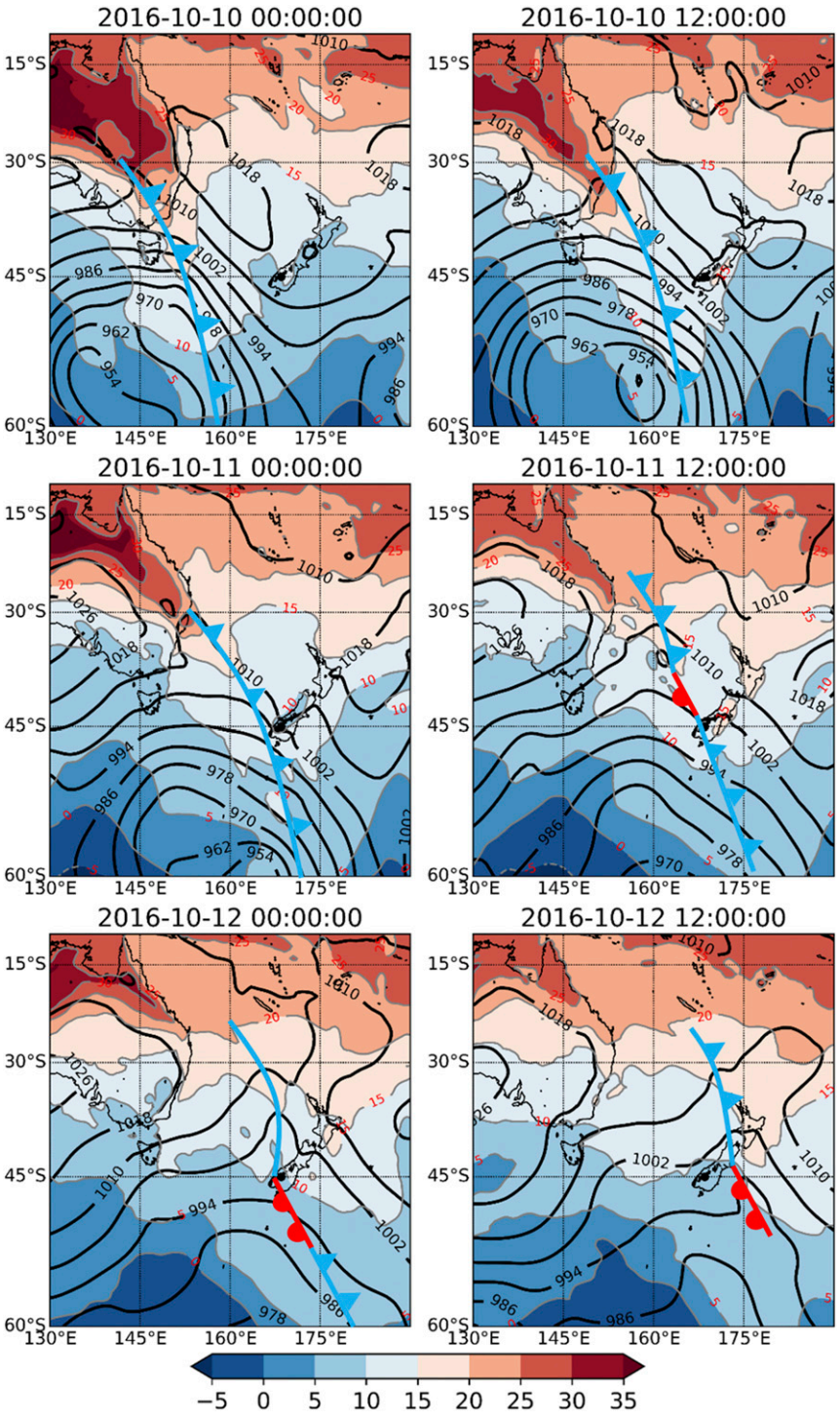

FIG. 7. Analysis maps of surface temperature T (°C) and SLP (hPa) during October 2016 event. The cold and warm fronts on the maps have been redrawn according to surface analysis maps of the Australian Bureau of Meteorology (from http://www.bom.gov.au/).

the world such as eastern Antarctica (Gorodetskaya et al. 2014), the western United states (Guan et al. 2013; Hansen 2016; Backes et al. 2015), and the South American Andes (Viale and Nuñez 2011; Saavedra et al. 2020), where a large fraction of total annual snow accumulation is received amidst the landfall of several ARs during a snow year. The magnitude of maximum IVT during the snowstorms rarely exceeds 600 $\mathrm{kg\,m^{-1}\,s^{-1}}$ along the west coast of the South Island, and the

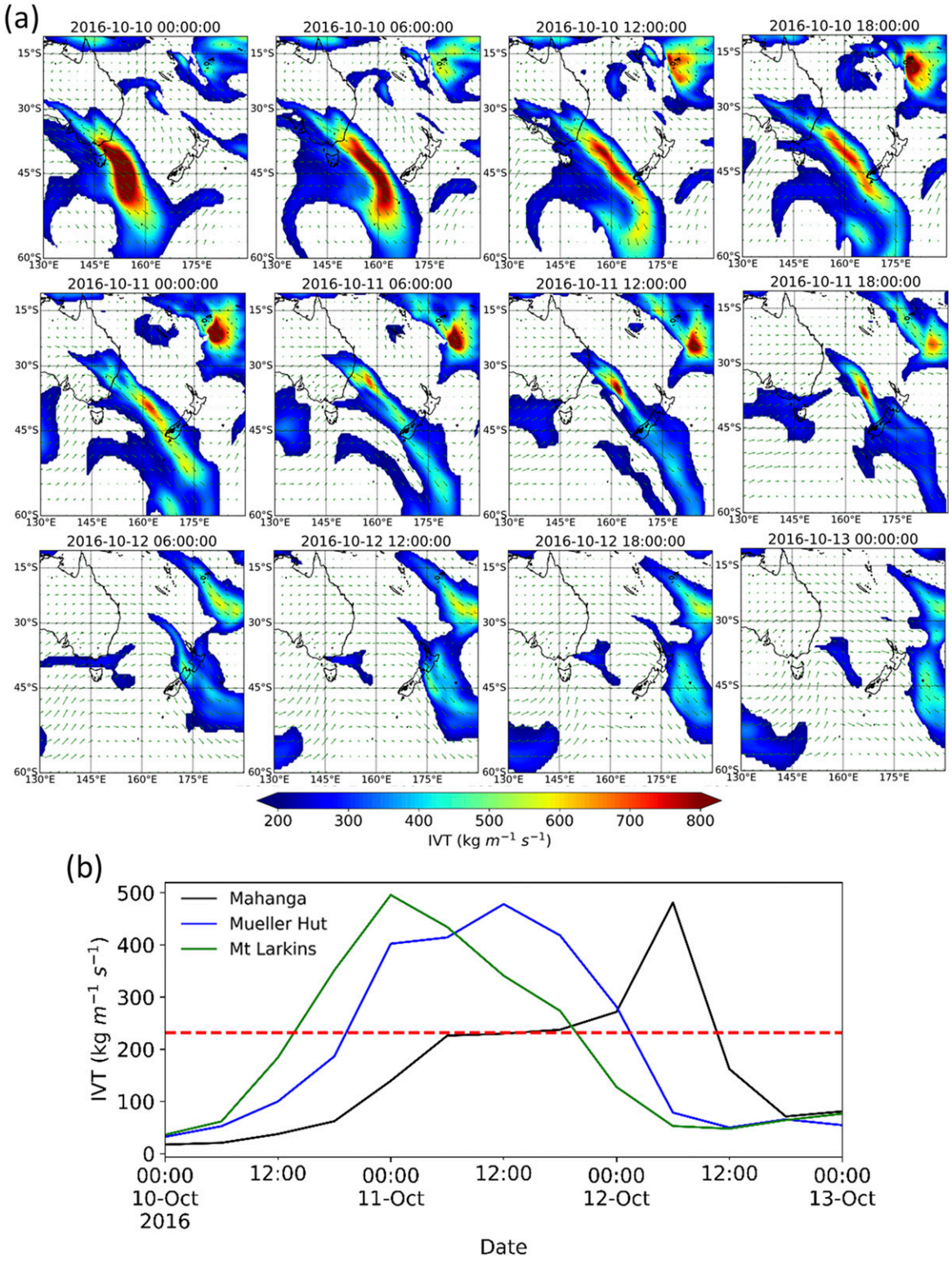

FIG. 8. (a) Six-hourly IVT (kg m^{-1} s^{-1}) during October 2016 snowstorm and (b) time series of 6-hourly IVT (kg m^{-1} s^{-1}) at three locations.

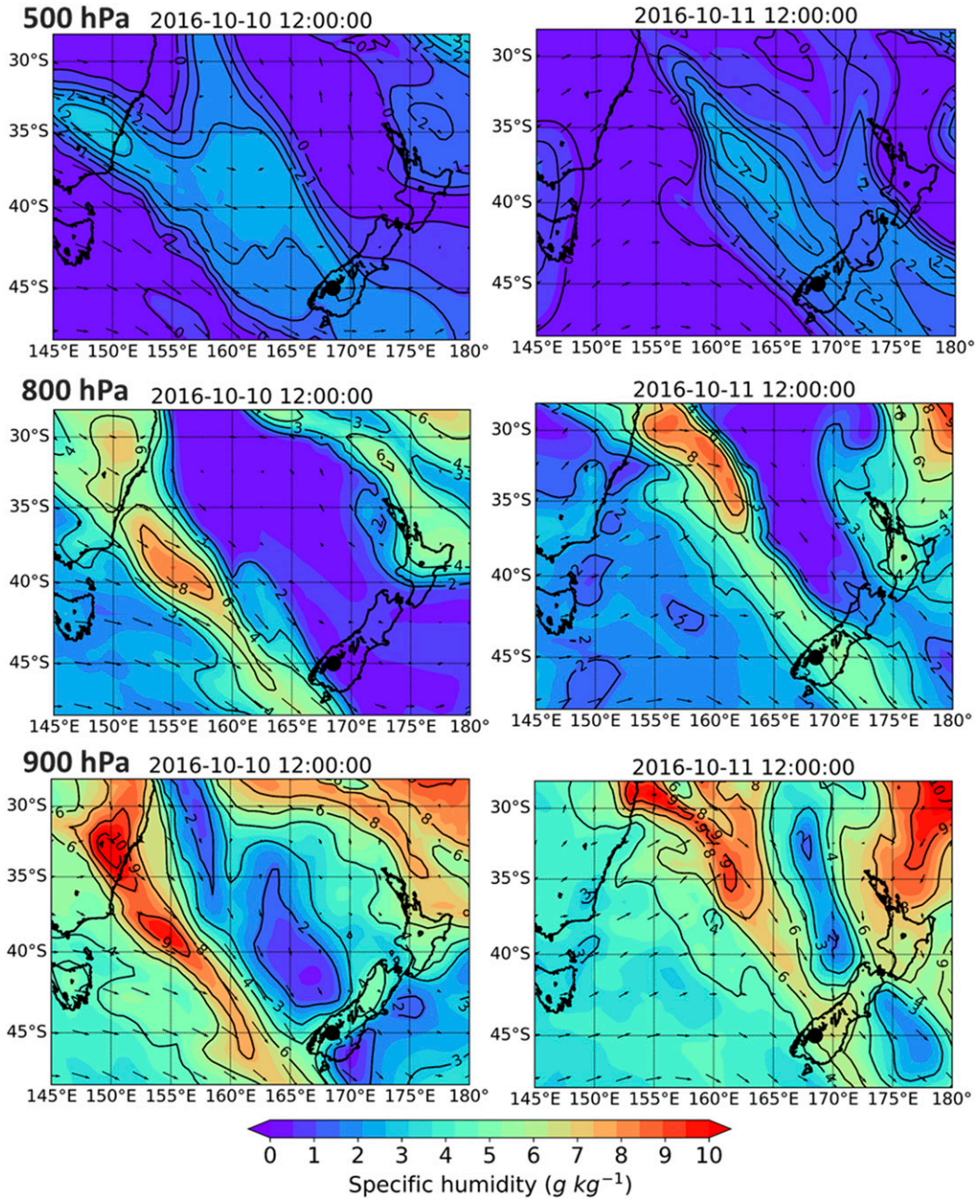

FIG. 9. Specific humidity and wind directions (black arrows) during the passage of AR over the South Island of New Zealand at three pressure levels (500, 800, and 900 hPa).

maximum IVT remains mainly just below 500 kg m^{-1} s^{-1} at the locations of the snow observations across the Southern Alps. These results are in broad consistency with a recent study by Little et al. (2019), who also reported IVT values between 250 and 500 kg m^{-1} s^{-1} associated with the five most extreme snowfall events on Brewster Glacier, located on the west flank of the Main Divide of the Southern Alps.

However, the IVT values calculated during large wintertime snowfall events in the Southern Alps are much lower than IVT values during flood-generating ARs in the New Zealand Southern Alps (Kingston et al. 2016) and other midlatitude regions such as western United States (Ralph et al. 2019; Dettinger et al. 2011; Neiman et al. 2013) and the United Kingdom (Lavers et al. 2012) where strong and persistent IVTs more than 1000 kg m^{-1} s^{-1} have been recorded during the major floods. Synoptic analysis of atmospheric conditions associated with a winter storm (11–12 October 2016) was conducted in order to shed more light on the key hydrometeorological characteristics of ARs in the maritime Southern Alps. The October event was an example of an AR responsible for both

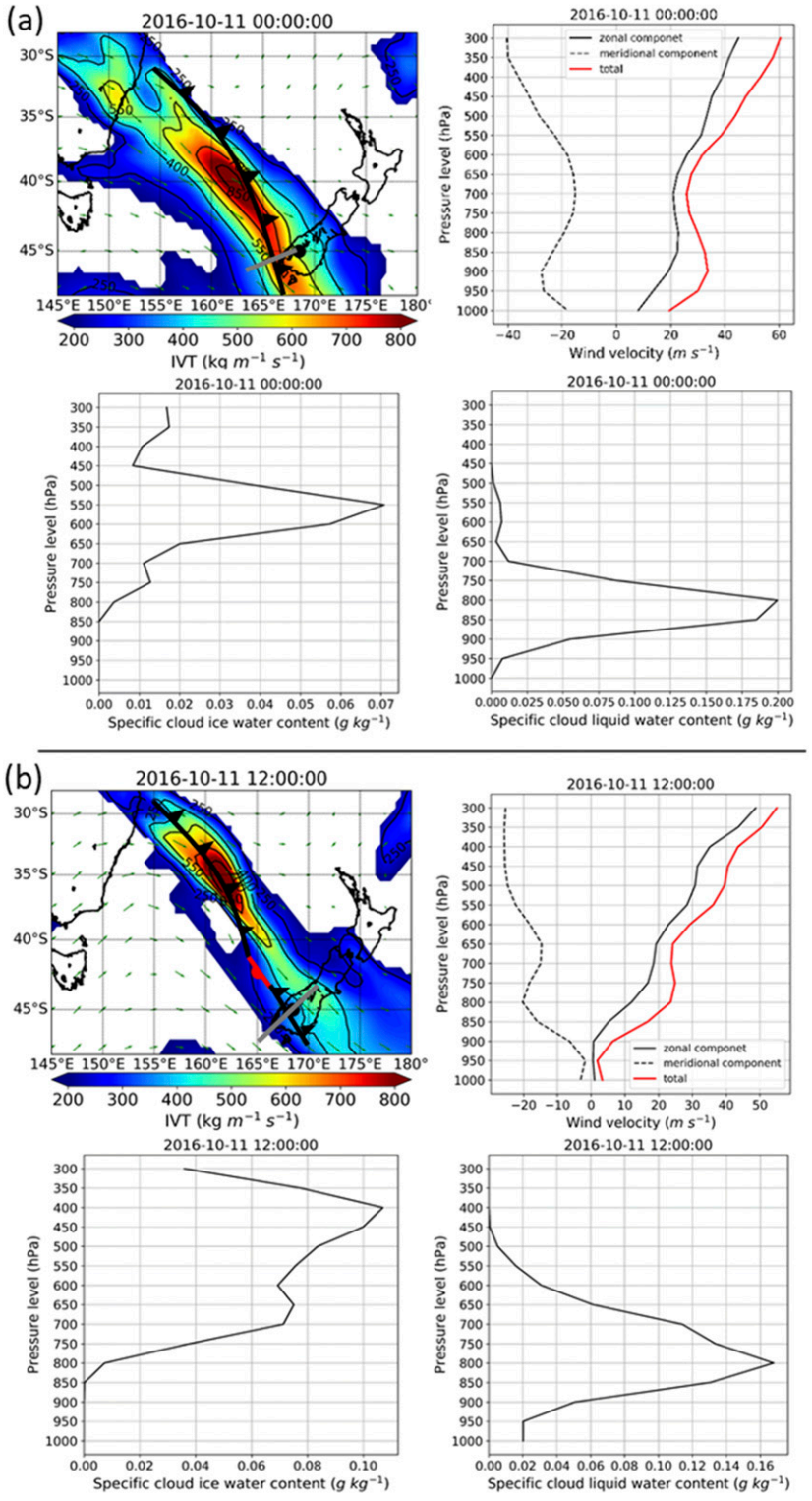

FIG. 10. Vertical profiles of specific cloud ice and liquid water content and wind components across the cold front for (a) 0000 NZST 11 Oct 2016 and (b) 1200 NZST 11 Oct 2016.

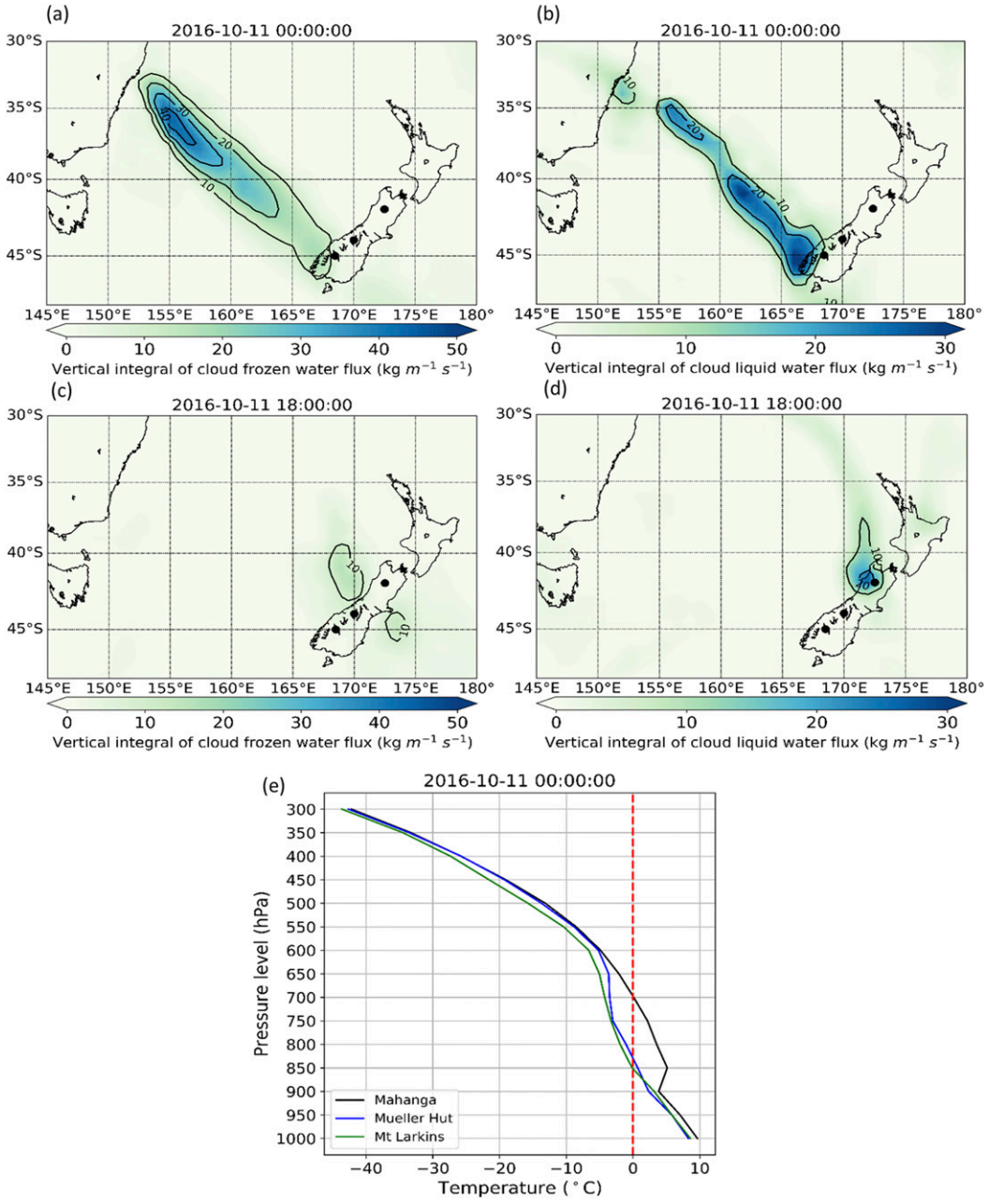

FIG. 11. (a) VICFWF and (b) VICLWF (kg m^{-1} s^{-1}) at 0000 NZST 11 Oct 2016. (c) VICFWF and (d) VICLWF (kg m^{-1} s^{-1}) at 1800 NZST 11 Oct 2016. (e) Vertical profile of temperature for pressure levels between 300 and 1000 hPa for the grid points of the study sites.

snow and rain at high altitudes. Strong fields of IVT within a northwesterly airflow and concomitant low pressure systems provided favorable conditions for heavy snowfall events in the Southern Alps. Additionally, exploring the vertical profiles of moisture transport across the cold front provide new insights to enhance our understanding of hydrometeorological attributes of a landfalling AR such as cloud water content and wind components. The consistency of presence of low- and midlevel moisture (below 500 hPa) and strong winds were identified during the passage of this AR over the Southern Alps (Fig. 9). The enhanced magnitudes of mid- and low-tropospheric specific humidity (>6 g kg^{-1} below 850 hPa) and strong wind velocities perpendicular to the Southern Alps resulted in an AR with northwesterly direction. This northwesterly airflow is analogous to those ARs associated with largest snowfall events recorded at in central and northern parts of the Southern Alps (Fig. 5). In addition, these characteristics of an AR-associated snowfall event over the Southern Alps are comparable to those findings

reported from other midlatitude regions such as Mount Shasta and the Sierra Nevada in California, United States (Hansen 2016; Backes et al. 2015), and the Central Andes (Viale and Nuñez 2011), where the low-level tropospheric water transport with a strong component of the meridional wind were distinctive characteristics of ARs responsible for extreme snowfall events. The vertical profiles across the cold front presented in this study (Fig. 10) highlights the key features of ARs (e.g., could water content and wind components) relative to the position of the cold fronts when they make landfall over a mountainous region.

The maritime characteristics of the New Zealand Southern Alps result in conditions where the snowfall events occur at temperatures close to freezing levels (Cullen and Conway 2015; Fitzharris et al. 1999). Even though the majority of AR-related winter storms investigated in this study produce large snowfall events at higher altitudes of the Southern Alps, the same weather systems concurrently could lead to heavy rainfall events at coastal regions on the west coast where they first make landfall over the New Zealand region. At high altitudes, however, the phase of the winter precipitation is largely influenced by the variations of the rain/snow transition line (Minder et al. 2011; Minder and Kingsmill 2013), where changes of a few hundreds of meters in the position of the transition from liquid to solid precipitation can significantly influence the precipitation type and hydrological processes in the alpine catchments (Minder 2010; White et al. 2002; Harpold et al. 2017; Harder and Pomeroy 2014). During October 2016 event, as the AR initially made landfall in the southwest of the South Island and then moved north, the position of the rain/snow transition and the cold front made a large distinction between precipitation type (solid or liquid) across the Southern Alps. While heavy snow fell at Mt Larkins and Mueller Hut during the passage of the AR, a shift from rain to snow occurred in the northern parts of the Southern Alps resulting in ROS at Mahanga. This is despite the fact that all three observation sites are located at somewhat similar altitudes. This highlights the importance of an accurate assessment of the rain/snow transition during winter precipitation in the maritime environments given the high sensitivity to small changes in temperature variations.

As this study focused on ARs associated with large snowfall events, a question remains about the frequency of wintertime ARs and their role in both annual snow accumulation and rainfall events. Investigating the association between the ARs and rainfall events in the Southern Alps during winter is important, for a higher frequency of wintertime ROS events has been projected in a warming climate where a shift from snow-dominated patterns to rain-dominated patterns is inevitable (Barnett et al. 2005; Bieniek et al. 2018; Cohen et al. 2015). Several studies have predicted significant changes across the globe in the trend and frequency of ARs due to a warming climate (Espinoza et al. 2018; Lavers et al. 2013, 2015). More frequent episodes of rain-generating ARs during winter and spring would largely impact the hydrological cycle by melting snow cover at higher rates resulting in the reduction of streamflow during spring (Surfleet and Tullos 2013; Cohen et al. 2015). The relatively warmer nature of ARs and their sensitivity to changes in temperature reported in similar midlatitude AR-affected regions such as western United States and South American Andes (Guan et al. 2016; Viale and Nuñez 2011; Dettinger 2011; Lavers et al. 2015) provide evidence that a warming climate can pose a major threat to the future of seasonal snowpacks at midlatitudes as more AR-related snowfall events would turn into rain events. In the Southern Alps, even though, previous studies have shown the frequent occurrence of winter ROS in the Southern Alps (Moore and Owens 1984); knowledge gaps have remained regarding the impacts of such events on alpine hydrology of the Southern Alps.

5. Summary and conclusions

It is generally understood that ARs are important in hydrological events in the midlatitude regions. In this study we focused on recognizing the role of ARs in solid precipitation of the Southern Alps. Daily snow observations from three locations across the Southern Alps were combined with atmospheric variables from ERA-Interim reanalysis data to investigate the moisture transport during large snowfall events. Comparing the average annual sum of large snow events with the total annual snow accumulation indicates that such events could account for up to 40% of the total snow accumulation throughout a snow year highlighting their relative importance in winter precipitation over the Southern Alps. The occurrence of snow events in the Southern Alps is significantly influenced by atmospheric forcing over the Tasman Sea. Strong fields of IVT responsible for moisture transport, accompanied by low pressure systems centered in west and southwest of the New Zealand's South Island are the main driver of large snowfall events over the Southern Alps. Our findings provided further evidence about the strong connection between wintertime large snowfall events and landfalling ARs in the Southern Alps, where a majority of such large snowfall events were resulted from narrow and strong moisture flux traveling across the Tasman Sea toward the Southern Alps. The frequent occurrence of ARs during large snow events across the Southern Alps indicates the key role of meridional water transport for precipitation. The moisture transport within a predominantly northwesterly airflow is a significant contributing component during large snowfall events. Analysis of vertical profiles shows that low- and midlevel jet streams play a critical role in transferring moisture across the South Pacific Ocean over Tasman Sea prior to large snowfall events in the Southern Alps. The close relationship between ARs and large snowfall events has implications on predictability of extreme winter precipitation in the Southern Alps. Since the position and strength of water vapor flux inside an AR impact the magnitude of incoming moisture available for precipitation, the findings of this study can be used to complement operational forecasting models for predicting large snow events in the maritime conditions.

Future work would address the frequency of wintertime ARs making landfall in the region and their potential role in producing rain rather than snow at higher altitudes. Investigating mesoscale characteristics of AR-related rain and snow storms in the Southern Alps could provide further knowledge about the impacts of large-scale circulation

patterns on physical processes controlling the precipitation type in the Southern Alps.

Acknowledgments. This work was carried out as part of the lead author's PhD research at University of Canterbury under UC Doctoral Scholarship. The authors thank Kathy Walter and Jeremy Rutherford from National Institute of Water and Atmospheric Research (NIWA) for help acquiring snow observations data from SIN database. We also thank the West Coast Regional Council for providing rainfall data at Hokitika Gorge and Cropp River rain gauges.

Data availability statement. The data that support the findings of this research are available from the corresponding author upon reasonable request.

REFERENCES

Backes, T. M., M. L. Kaplan, R. Schumer, and J. F. Mejia, 2015: A climatology of the vertical structure of water vapor transport to the Sierra Nevada in cool season Atmospheric River precipitation events. *J. Hydrometeor.*, **16**, 1029–1047, https://doi.org/10.1175/JHM-D-14-0077.1.

Bao, J.-W., S. A. Michelson, P. J. Neiman, F. M. Ralph, and J. M. Wilczak, 2006: Interpretation of enhanced integrated water vapor bands associated with extratropical cyclones: Their formation and connection to tropical moisture. *Mon. Wea. Rev.*, **134**, 1063–1080, https://doi.org/10.1175/MWR3123.1.

Barnett, T. P., J. C. Adam, and D. P. Lettenmaier, 2005: Potential impacts of a warming climate on water availability in snow-dominated regions. *Nature*, **438**, 303–309, https://doi.org/10.1038/nature04141.

Bednorz, E., 2011: Synoptic conditions of the occurrence of snow cover in central European lowlands. *Int. J. Climatol.*, **31**, 1108–1118, https://doi.org/10.1002/joc.2130.

——, and J. Wibig, 2016: Spatial distribution and synoptic conditions of snow accumulation in the Russian Arctic. *Polar Res.*, **35**, 25916, https://doi.org/10.3402/polar.v35.25916.

Benedict, I., K. Ødemark, T. Nipen, and R. Moore, 2019: Large-scale flow patterns associated with extreme precipitation and atmospheric rivers over Norway. *Mon. Wea. Rev.*, **147**, 1415–1428, https://doi.org/10.1175/MWR-D-18-0362.1.

Bieniek, P. A., U. S. Bhatt, J. E. Walsh, R. Lader, B. Griffith, J. K. Roach, and R. L. Thoman, 2018: Assessment of Alaska rain-on-snow events using dynamical downscaling. *J. Appl. Meteor. Climatol.*, **57**, 1847–1863, https://doi.org/10.1175/JAMC-D-17-0276.1.

Birkeland, K. W., and C. J. Mock, 1996: Atmospheric circulation patterns associated with heavy snowfall events, Bridger Bowl, Montana, U.S.A. *Mt. Res. Dev.*, **16**, 281, https://doi.org/10.2307/3673951.

Brandolino, C., 2016a: Climate summary for July 2016. NIWA, https://niwa.co.nz/climate/summaries/monthly/climate-summary-for-july-2016.

——, 2016b: Climate summary for October 2016. NIWA, https://niwa.co.nz/climate/summaries/monthly/climate-summary-for-october-2016.

Clark, M. P., and Coauthors, 2009: Simulations of seasonal snow for the south Island, New Zealand. *J. Hydrol. N.Z.*, **48**, 41–58.

——, and Coauthors, 2011: Representing spatial variability of snow water equivalent in hydrologic and land-surface models: A review. *Water Resour. Res.*, **47**, W07539, https://doi.org/10.1029/2011WR010745.

Cohen, J., H. Ye, and J. Jones, 2015: Trends and variability in rain-on-snow events. *Geophys. Res. Lett.*, **42**, 7115–7122, https://doi.org/10.1002/2015GL065320.

Cordeira, J. M., F. M. Ralph, A. Martin, N. Gaggini, J. R. Spackman, P. J. Neiman, J. J. Rutz, and R. Pierce, 2017: Forecasting Atmospheric Rivers during CalWater 2015. *Bull. Amer. Meteor. Soc.*, **98**, 449–459, https://doi.org/10.1175/BAMS-D-15-00245.1.

Cullen, N. J., and J. P. Conway, 2015: A 22 month record of surface meteorology and energy balance from the ablation zone of Brewster Glacier, New Zealand. *J. Glaciol.*, **61**, 931–946, https://doi.org/10.3189/2015JoG15J004.

——, P. B. Gibson, T. Mölg, J. P. Conway, P. Sirguey, and D. G. Kingston, 2019: The influence of weather systems in controlling mass balance in the Southern Alps of New Zealand. *J. Geophys. Res. Atmos.*, **124**, 4514–4529, https://doi.org/10.1029/2018JD030052.

Daniel, J. S., S. Solomon, R. W. Portmann, A. O. Langford, C. S. Eubank, E. G. Dutton, and W. Madsen, 2002: Cloud liquid water and ice measurements from spectrally resolved near-infrared observations: A new technique. *J. Geophys. Res. Atmos.*, **107**, 4599, https://doi.org/10.1029/2001JD000688..

Dean, S., B. A. Mullan, and J. Renwick, 2006: More shorts and gumboots? New Zealand climate at the end of this century as simulated by a regional climate model. *Resource Management under Stormy Skies: Water Allocation at the Crossroads*, New Zealand Hydrological Society.

Dee, D. P., and Coauthors, 2011: The ERA-Interim reanalysis: Configuration and performance of the data assimilation system. *Quart. J. Roy. Meteor. Soc.*, **137**, 553–597, https://doi.org/10.1002/qj.828.

Demaria, E. M. C. C., F. Dominguez, H. Hu, G. von Glinski, M. Robles, J. Skindlov, and J. Walter, 2017: Observed hydrologic impacts of landfalling atmospheric rivers in the Salt and Verde River basins of Arizona, United States. *Water Resour. Res.*, **53**, 10 025–10 042, https://doi.org/10.1002/2017WR020778.

Dettinger, M., 2011: Climate change, atmospheric rivers, and floods in California - A multimodel analysis of storm frequency and magnitude changes. *J. Amer. Water Resour. Assoc.*, **47**, 514–523, https://doi.org/10.1111/j.1752-1688.2011.00546.x.

Dettinger, M. D., 2013: Atmospheric rivers as drought busters on the U.S. West Coast. *J. Hydrometeor.*, **14**, 1721–1732, https://doi.org/10.1175/JHM-D-13-02.1.

——, F. M. Ralph, T. Das, P. J. Neiman, and D. R. Cayan, 2011: Atmospheric rivers, floods and the water resources of California. *Water*, **3**, 445–478, https://doi.org/10.3390/w3020445.

Dirmeyer, P. A., and J. L. Kinter, 2009: The "Maya Express": Floods in the U.S. Midwest. *Eos, Trans. Amer. Geophys. Union*, **90**, 101–102, https://doi.org/10.1029/2009EO120001.

Eckhardt, S., A. Stohl, H. Wernli, P. James, C. Forster, and N. Spichtinger, 2004: A 15-year climatology of warm conveyor belts. *J. Climate*, **17**, 218–237, https://doi.org/10.1175/1520-0442(2004)017<0218:AYCOWC>2.0.CO;2.

Espinoza, V., D. E. Waliser, B. Guan, D. A. Lavers, and F. M. Ralph, 2018: Global analysis of climate change projection effects on atmospheric rivers. *Geophys. Res. Lett.*, **45**, 4299–4308, https://doi.org/10.1029/2017GL076968.

Fitzharris, B., W. Lawson, and I. Owens, 1999: Research on glaciers and snow in New Zealand. *Prog. Phys. Geogr.*, **23**, 469–500, https://doi.org/10.1177/030913339902300402.

Fitzharris, B. B., and C. E. Garr, 1995: Simulation of past variability in seasonal snow in the Southern Alps, New Zealand. *Ann. Glaciol.*, **21**, 377–382, https://doi.org/10.3189/S0260305500016098.

Gimeno, L., R. Nieto, M. Vázquez, and D. A. Lavers, 2014: Atmospheric rivers: A mini-review. *Front. Earth Sci.*, **2**, 1–6, https://doi.org/10.3389/feart.2014.00002.

Gorodetskaya, I. V., M. Tsukernik, K. Claes, M. F. Ralph, W. D. Neff, and N. P. M. Van Lipzig, 2014: The role of atmospheric rivers in anomalous snow accumulation in East Antarctica. *Geophys. Res. Lett.*, **41**, 6199–6206, https://doi.org/10.1002/2014GL060881.

Griffiths, G. A., and M. J. Mcsaveney, 1983: Distribution of mean annual precipitation across some steepland regions of New Zealand. *N. Z. J. Sci.*, **26**, 197–209.

Guan, B., and D. E. Waliser, 2015: Detection of atmospheric rivers: Evaluation and application of an algorithm for global studies. *J. Geophys. Res. Atmos.*, **120**, 12 514–12 535, https://doi.org/10.1002/2015JD024257.

——, N. P. Molotch, D. E. Waliser, E. J. Fetzer, and P. J. Neiman, 2010: Extreme snowfall events linked to atmospheric rivers and surface air temperature via satellite measurements. *Geophys. Res. Lett.*, **37**, L20401, https://doi.org/10.1029/2010GL044696.

——, D. E. Waliser, N. P. Molotch, E. J. Fetzer, and P. J. Neiman, 2012: Does the Madden–Julian oscillation influence wintertime atmospheric rivers and snowpack in the Sierra Nevada? *Mon. Wea. Rev.*, **140**, 325–342, https://doi.org/10.1175/MWR-D-11-00087.1.

——, N. P. Molotch, D. E. Waliser, E. J. Fetzer, and P. J. Neiman, 2013: The 2010/2011 snow season in California's Sierra Nevada: Role of atmospheric rivers and modes of large-scale variability. *Water Resour. Res.*, **49**, 6731–6743, https://doi.org/10.1002/wrcr.20537.

——, D. E. Waliser, F. M. Ralph, E. J. Fetzer, and P. J. Neiman, 2016: Hydrometeorological characteristics of rain-on-snow events associated with atmospheric rivers. *Geophys. Res. Lett.*, **43**, 2964–2973, https://doi.org/10.1002/2016GL067978.

Hansen, C., 2016: Diagnosing the role of atmospheric rivers, past and present, in snowfall events on Mt. Shasta, California. Ph.D. thesis, University of Nevada, Reno, 200 pp., http://hdl.handle.net/11714/2201.

——, M. Kaplan, S. Mensing, S. Underwood, J. Lewis, K. King, and J. Haugland, 2013: They just don't make storms like this one anymore: Analyzing the anomalous record snowfall event of 1959. *J. Operat. Meteor.*, **1**, 52–65, https://doi.org/10.15191/nwajom.2013.0105.

Harder, P., and J. W. Pomeroy, 2014: Hydrological model uncertainty due to precipitation-phase partitioning methods. *Hydrol. Processes*, **28**, 4311–4327, https://doi.org/10.1002/hyp.10214.

Harpold, A. A., M. L. Kaplan, P. Z. Klos, T. Link, J. P. McNamara, S. Rajagopal, R. Schumer, and C. M. Steele, 2017: Rain or snow: hydrologic processes, observations, prediction, and research needs. *Hydrol. Earth Syst. Sci.*, **21**, 1–22, https://doi.org/10.5194/hess-21-1-2017.

Henderson, R. D., and S. M. Thosmson, 1999: Extreme rainfalls in the Southern Alps of New Zealand. *J. Hydrol. N.Z.*, **38**, 309–330.

Hendrikx, J., E. Ö. Hreinsson, M. P. Clark, and A. B. Mullan, 2012: The potential impact of climate change on seasonal snow in New Zealand: Part I—An analysis using 12 GCMs. *Theor. Appl. Climatol.*, **110**, 607–618, https://doi.org/10.1007/s00704-012-0711-1.

Huning, L. S., S. A. Margulis, B. Guan, D. E. Waliser, and P. J. Neiman, 2017: Implications of detection methods on characterizing atmospheric river contribution to seasonal snowfall across Sierra Nevada, USA. *Geophys. Res. Lett.*, **44**, 10 445–10 453, https://doi.org/10.1002/2017GL075201.

——, B. Guan, D. E. Waliser, and D. P. Lettenmaier, 2019: Sensitivity of seasonal snowfall attribution to atmospheric rivers and their reanalysis-based detection. *Geophys. Res. Lett.*, **46**, 794–803, https://doi.org/10.1029/2018GL080783.

Jobst, A. M., D. G. Kingston, N. J. Cullen, and J. Schmid, 2018: Intercomparison of different uncertainty sources in hydrological climate change projections for an alpine catchment (Upper Clutha River, New Zealand). *Hydrol. Earth Syst. Sci.*, **22**, 3125–3142, https://doi.org/10.5194/hess-22-3125-2018.

Junker, N. W., R. H. Grumm, R. Hart, L. F. Bosart, K. M. Bell, and F. J. Pereira, 2008: Use of normalized anomaly fields to anticipate extreme rainfall in the mountains of Northern California. *Wea. Forecast.*, **23**, 336–356, https://doi.org/10.1175/2007WAF2007013.1.

Kerr, T., 2013: The contribution of snowmelt to the rivers of the South Island, New Zealand. *J. Hydrol. N.Z.*, **52**, 61–82.

——, M. Clark, J. Hendrikx, and B. Anderson, 2013: Snow distribution in a steep mid-latitude alpine catchment. *Adv. Water Resour.*, **55**, 17–24, https://doi.org/10.1016/j.advwatres.2012.12.010.

Khain, A. P., and M. Pinsky, 2018: *Physical Processes in Clouds and Cloud Modeling*. Cambridge University Press, 640 pp.

Kingston, D. G., D. A. Lavers, and D. M. Hannah, 2016: Floods in the Southern Alps of New Zealand: The importance of atmospheric rivers. *Hydrol. Processes*, **30**, 5063–5070, https://doi.org/10.1002/hyp.10982.

Lackmann, G. M., and J. R. Gyakum, 1999: Heavy cold-season precipitation in the northwestern United States: Synoptic climatology and an analysis of the flood of 17–18 January 1986. *Wea. Forecasting*, **14**, 687–700, https://doi.org/10.1175/1520-0434(1999)014<0687:HCSPIT>2.0.CO;2.

Lavers, D. A., and G. Villarini, 2013: The nexus between atmospheric rivers and extreme precipitation across Europe. *Geophys. Res. Lett.*, **40**, 3259–3264, https://doi.org/10.1002/grl.50636.

——, ——, R. P. Allan, E. F. Wood, and A. J. Wade, 2012: The detection of atmospheric rivers in atmospheric reanalyses and their links to British winter floods and the large-scale climatic circulation. *J. Geophys. Res.*, **117**, D20106, https://doi.org/10.1029/2012JD018027.

——, R. P. Allan, G. Villarini, B. Lloyd-Hughes, D. J. Brayshaw, and A. J. Wade, 2013: Future changes in atmospheric rivers and their implications for winter flooding in Britain. *Environ. Res. Lett.*, **8**, 034010, https://doi.org/10.1088/1748-9326/8/3/034010.

——, F. M. Ralph, D. E. Waliser, A. Gershunov, and M. D. Dettinger, 2015: Climate change intensification of horizontal water vapor transport in CMIP5. *Geophys. Res. Lett.*, **42**, 5617–5625, https://doi.org/10.1002/2015GL064672.

Leung, L. R., and Y. Qian, 2009: Atmospheric rivers induced heavy precipitation and flooding in the western U.S. simulated by the WRF regional climate model. *Geophys. Res. Lett.*, **36**, L03820, https://doi.org/10.1029/2008GL036445..

Little, K., D. G. Kingston, N. J. Cullen, and P. B. Gibson, 2019: The role of atmospheric rivers for extreme ablation and snowfall events in the Southern Alps of New Zealand. *Geophys. Res. Lett.*, **46**, 2761–2771, https://doi.org/10.1029/2018GL081669.

Lu, M., and U. Lall, 2016: Tropical moisture exports, extreme precipitation and floods in northeast US. *Hydrol. Earth Syst. Sci. Discuss.*, https://doi.org/10.5194/hess-2016-403.

Lute, A. C., and J. T. Abatzoglou, 2014: Role of extreme snowfall events in interannual variability of snowfall accumulation in the western United States. *Water Resour. Res.*, **50**, 2874–2888, https://doi.org/10.1002/2013WR014465.

McKerchar, A. I., C. P. Pearson, and B. B. Fitzharris, 1998: Dependency of summer lake inflows and precipitation on spring SOI. *J. Hydrol.*, **205**, 66–80, https://doi.org/10.1016/S0022-1694(97)00144-3.

Merino, A., S. Fernández, L. Hermida, L. López, J. L. Sánchez, E. García-Ortega, and E. Gascón, 2014: Snowfall in the northwest Iberian Peninsula: Synoptic circulation patterns and their influence on snow day trends. *Sci. World J.*, **2014**, 480275, https://doi.org/10.1155/2014/480275.

Minder, J. R., 2010: The sensitivity of mountain snowpack accumulation to climate warming. *J. Climate*, **23**, 2634–2650, https://doi.org/10.1175/2009JCLI3263.1.

——, and D. E. Kingsmill, 2013: Mesoscale variations of the atmospheric snow line over the northern Sierra Nevada: Multiyear statistics, case study, and mechanisms. *J. Atmos. Sci.*, **70**, 916–938, https://doi.org/10.1175/JAS-D-12-0194.1.

——, D. R. Durran, and G. H. Roe, 2011: Mesoscale controls on the mountainside snow line. *J. Atmos. Sci.*, **68**, 2107–2127, https://doi.org/10.1175/JAS-D-10-05006.1.

Molero, G. C., and Y. S. Novelli, 2019: The role of atmospheric-tropospheric rivers in partitioning coastal habitats and limiting the poleward expansion of mangroves along the southeast coast of Brazil. *Int. J. Hydrol.*, **3**, 92–94, https://doi.org/10.15406/ijh.2019.03.00168.

Moore, R. D., and I. F. Owens, 1984: Controls on advective snowmelt in a Maritime Alpine Basin. *J. Climate Appl. Meteor.*, **23**, 135–142, https://doi.org/10.1175/1520-0450(1984)023<0135:COASIA>2.0.CO;2.

Neiman, P. J., F. M. Ralph, G. A. Wick, Y.-H. H. Kuo, T.-K. K. Wee, Z. Ma, G. H. Taylor, and M. D. Dettinger, 2008a: Diagnosis of an intense atmospheric river impacting the Pacific Northwest: Storm summary and offshore vertical structure observed with COSMIC satellite retrievals. *Mon. Wea. Rev.*, **136**, 4398–4420, https://doi.org/10.1175/2008MWR2550.1.

——, ——, ——, J. D. Lundquist, and M. D. Dettinger, 2008b: Meteorological characteristics and overland precipitation impacts of atmospheric rivers affecting the West Coast of North America based on eight years of SSM/I satellite observations. *J. Hydrometeor.*, **9**, 22–47, https://doi.org/10.1175/2007JHM855.1.

——, and Coauthors, 2013: The landfall and inland penetration of a flood-producing atmospheric river in Arizona. Part I: Observed synoptic-scale, orographic, and hydrometeorological characteristics. *J. Hydrometeor.*, **14**, 460–484, https://doi.org/10.1175/JHM-D-12-0101.1.

Newell, R. E., N. E. Newell, Y. Zhu, and C. Scott, 1992: Tropospheric rivers? - A pilot study. *Geophys. Res. Lett.*, **19**, 2401–2404, https://doi.org/10.1029/92GL02916.

Poyck, S., and Coauthors, 2011: Combined snow and streamflow modelling to estimate impacts of climate change on water resources in the Clutha River, New Zealand. *J. Hydrol. N.Z.*, **50**, 293–311.

Purdie, H., A. Mackintosh, W. Lawson, and B. Anderson, 2011: Synoptic influences on snow accumulation on glaciers east and west of a topographic divide: Southern Alps, New Zealand. *Arct. Antarct. Alp. Res.*, **43**, 82–94, https://doi.org/10.1657/1938-4246-43.1.82.

Ralph, F. M., P. J. Neiman, and G. A. Wick, 2004: Satellite and CALJET aircraft observations of atmospheric rivers over the eastern North Pacific Ocean during the winter of 1997/98. *Mon. Wea. Rev.*, **132**, 1721–1745, https://doi.org/10.1175/1520-0493(2004)132<1721:SACAOO>2.0.CO;2.

——, and Coauthors, 2016: CalWater field studies designed to quantify the roles of atmospheric rivers and aerosols in modulating U.S. West Coast precipitation in a changing climate. *Bull. Amer. Meteor. Soc.*, **97**, 1209–1228, https://doi.org/10.1175/BAMS-D-14-00043.1.

——, and Coauthors, 2017: Atmospheric rivers emerge as a global science and applications focus. *Bull. Amer. Meteor. Soc.*, **98**, 1969–1973, https://doi.org/10.1175/BAMS-D-16-0262.1.

——, J. J. Rutz, J. M. Cordeira, M. Dettinger, M. Anderson, D. Reynolds, L. J. Schick, and C. Smallcomb, 2019: A scale to characterize the strength and impacts of atmospheric rivers. *Bull. Amer. Meteor. Soc.*, **100**, 269–289, https://doi.org/10.1175/BAMS-D-18-0023.1.

Rössler, O., P. Froidevaux, U. Börst, R. Rickli, O. Martius, and R. Weingartner, 2014: Retrospective analysis of a nonforecasted rain-on-snow flood in the Alps – A matter of model limitations or unpredictable nature? *Hydrol. Earth Syst. Sci.*, **18**, 2265–2285, https://doi.org/10.5194/hess-18-2265-2014.

Rutz, J. J., and Coauthors, 2014: Climatological characteristics of atmospheric rivers and their inland penetration over the western United States. *Mon. Wea. Rev.*, **142**, 905–921, https://doi.org/10.1175/MWR-D-13-00168.1.

——, and Coauthors, 2019: The Atmospheric River Tracking Method Intercomparison Project (ARTMIP): Quantifying uncertainties in atmospheric river climatology. *J. Geophys. Res. Atmos.*, **124**, 13 777–13 802, https://doi.org/10.1029/2019JD030936.

Saavedra, F., G. Cortés, M. Viale, S. Margulis, and J. McPhee, 2020: Atmospheric rivers contribution to the snow accumulation over the Southern Andes (26.5°S–37.5°S). *Front. Earth Sci.*, **8**, 261, https://doi.org/10.3389/feart.2020.00261.

Schumacher, B., M. Katurji, H. Meyer, T. Appelhans, I. Otte, and T. Nauss, 2020: Atmospheric moisture pathways of East Africa and implications for water recycling at Mount Kilimanjaro. *Int. J. Climatol.*, **40**, 4477–4496, https://doi.org/10.1002/joc.6468..

Shields, C. A., and Coauthors, 2018: Atmospheric River Tracking Method Intercomparison Project (ARTMIP): Project goals and experimental design. *Geosci. Model Dev.*, **11**, 2455–2474, https://doi.org/10.5194/gmd-11-2455-2018.

Sirguey, P., 2009: Monitoring snow cover and modelling catchment discharge with remote sensing in the Upper Waitaki Basin. Ph. D. thesis, School of Surveying, University of Otago, 436 pp.

Stohl, A., C. Forster, and H. Sodemann, 2008: Remote sources of water vapor forming precipitation on the Norwegian west coast at 60°N—A tale of hurricanes and an atmospheric river. *J. Geophys. Res.*, **113**, D05102, https://doi.org/10.1029/2007JD009006..

Surfleet, C. G., and D. Tullos, 2013: Variability in effect of climate change on rain-on-snow peak flow events in a temperate climate. *J. Hydrol.*, **479**, 24–34, https://doi.org/10.1016/j.jhydrol.2012.11.021.

Thompson, S. M., 2002: River discharge from mountains with frequent rain. *J. Hydrol. N.Z.*, **41**, 125–144.

Viale, M., and M. N. Nuñez, 2011: Climatology of winter orographic precipitation over the subtropical central andes and associated synoptic and regional characteristics. *J. Hydrometeor.*, **12**, 481–507, https://doi.org/10.1175/2010JHM1284.1.

——, R. Valenzuela, R. D. Garreaud, and F. M. Ralph, 2018: Impacts of atmospheric rivers on precipitation in southern

South America. *J. Hydrometeor.*, **19**, 1671–1687, https://doi.org/10.1175/JHM-D-18-0006.1.

Vicente-Serrano, S. M., and Coauthors, 2017: Extreme hydrological events and the influence of reservoirs in a highly regulated river basin of northeastern Spain. *J. Hydrol. Reg. Stud.*, **12**, 13–32, https://doi.org/10.1016/j.ejrh.2017.01.004.

Waliser, D., and B. Guan, 2017: Extreme winds and precipitation during landfall of atmospheric rivers. *Nat. Geosci.*, **10**, 179–183, https://doi.org/10.1038/ngeo2894.

Webster, C. S., D. G. Kingston, and T. Kerr, 2015: Inter-annual variation in the topographic controls on catchment-scale snow distribution in a maritime alpine catchment, New Zealand. *Hydrol. Processes*, **29**, 1096–1109, https://doi.org/10.1002/hyp.10224.

Whan, K., J. Sillmann, N. Schaller, and R. Haarsma, 2020: Future changes in atmospheric rivers and extreme precipitation in Norway. *Climate Dyn.*, **54**, 2071–2084, https://doi.org/10.1007/s00382-019-05099-z.

White, A. B., D. J. Gottas, E. T. Strem, F. M. Ralph, and P. J. Neiman, 2002: An automated brightband height detection algorithm for use with doppler radar spectral moments. *J. Atmos. Oceanic Technol.*, **19**, 687–697, https://doi.org/10.1175/1520-0426(2002)019<0687:AABHDA>2.0.CO;2.

Young, A. M., K. T. Skelly, and J. M. Cordeira, 2017: High-impact hydrologic events and atmospheric rivers in California: An investigation using the NCEI storm events database. *Geophys. Res. Lett.*, **44**, 3393–3401, https://doi.org/10.1002/2017GL073077.

Zhu, Y., and R. E. Newell, 1998: A proposed algorithm for moisture fluxes from atmospheric rivers. *Mon. Wea. Rev.*, **126**, 725–735, https://doi.org/10.1175/1520-0493(1998)126<0725:APAFMF>2.0.CO;2.